

## Manuscript Details

<b>Manuscript number</b>	DSR2_2017_17
<b>Title</b>	Characteristics and transformation of Pacific winter water on the Chukchi Sea shelf in late-spring
<b>Article type</b>	Full length article

### Abstract

Data from a late-spring survey of the northeast Chukchi Sea are used to investigate various aspects of the newly ventilated winter water (NVWW). More than 96% of the water sampled on the shelf was NVWW, the saltiest (densest) of which tended to be in the main flow pathways on the shelf. Nearly all of the hydrographic profiles on the shelf displayed a two-layer structure, with a surface mixed layer and bottom boundary layer separated by a weak density interface. Using a polynya model driven by realistic atmospheric forcing, together with a one-dimensional mixed layer model, we show that nearly all of the hydrographic profiles would become completely homogenized in less than a day as a result of brine rejection due to ice formation. Since the study domain was filled with leads within the pack ice – many of them re-freezing – and since some of the measured profiles were vertically uniform in density, this suggests that NVWW is formed throughout the Chukchi shelf via convection within small openings in the ice. This is consistent with the result that the salinity signals of the NVWW along the central shelf pathway cannot be explained solely by advection from Bering Strait or via modification within large polynyas. The local convection would be expected to stir nutrients into the water column from the sediments, which explains the high nitrate concentrations observed throughout the shelf. The atmospheric circulation during the latter half of the cruise caused air temperatures in the Chukchi Sea to be anomalously cold compared to climatology, which likely delayed the formation of melt ponds. This could explain why no under-ice phytoplankton blooms were observed during the cruise, despite the high levels of nitrate on the shelf.

<b>Corresponding Author</b>	Astrid Pacini
<b>Corresponding Author's Institution</b>	Woods Hole Oceanographic Institution
<b>Order of Authors</b>	Astrid Pacini, Robert Pickart, Kent Moore, Carolina Nobre, Frank Bahr, Kjetil Våge, Kevin Arrigo

## Submission Files Included in this PDF

### File Name [File Type]

pacini\_et al.pdf [Manuscript File]

To view all the submission files, including those not included in the PDF, click on the manuscript title on your EVISE Homepage, then click 'Download zip file'.

# **Characteristics and transformation of Pacific winter water on the Chukchi Sea shelf in late-spring**

Astrid Pacini<sup>1,2</sup>, Robert S. Pickart<sup>1</sup>, G.W.K. Moore<sup>3</sup>, C. Nobre<sup>1</sup>,

Frank Bahr<sup>1</sup>, K. Våge<sup>4</sup>, and Kevin R. Arrigo<sup>5</sup>

In preparation for Deep-Sea Research II, February 2017

Corresponding Author: A. Pacini ([apacini@whoi.edu](mailto:apacini@whoi.edu))

---

<sup>1</sup>Woods Hole Oceanographic Institution; Woods Hole, MA, USA.

<sup>2</sup>MIT/WHOI Joint program in Physical Oceanography; Woods Hole, MA, USA

<sup>3</sup>Department of Physics, University of Toronto; Toronto, Ontario, Canada

<sup>4</sup>Geophysical Institute, University of Bergen and Bjerknes Centre for Climate Research, Bergen, Norway

<sup>5</sup>Department of Environmental Earth System Science, Stanford University, Stanford, CA, USA

## **Abstract**

Data from a late-spring survey of the northeast Chukchi Sea are used to investigate various aspects of the newly ventilated winter water (NVWW). More than 96% of the water sampled on the shelf was NVWW, the saltiest (densest) of which tended to be in the main flow pathways on the shelf. Nearly all of the hydrographic profiles on the shelf displayed a two-layer structure, with a surface mixed layer and bottom boundary layer separated by a weak density interface. Using a polynya model driven by realistic atmospheric forcing, together with a one-dimensional mixed layer model, we show that nearly all of the hydrographic profiles would become completely homogenized in less than a day as a result of brine rejection due to ice formation. Since the study domain was filled with leads within the pack ice – many of them re-freezing – and since some of the measured profiles were vertically uniform in density, this suggests that NVWW is formed throughout the Chukchi shelf via convection within small openings in the ice. This is consistent with the result that the salinity signals of the NVWW along the central shelf pathway cannot be explained solely by advection from Bering Strait or via modification within large polynyas. The local convection would be expected to stir nutrients into the water column from the sediments, which explains the high nitrate concentrations observed throughout the shelf. The atmospheric circulation during the latter half of the cruise caused air temperatures in the Chukchi Sea to be anomalously cold compared to climatology, which likely delayed the formation of melt ponds. This could explain why no under-ice phytoplankton blooms were observed during the cruise, despite the high levels of nitrate on the shelf.

## 1. Introduction

The cold and dense winter water that flows northward through the Chukchi Sea each year is critical to the functioning of the ecosystem of the western Arctic Ocean. The high nutrient content of the water spurs primary production both on the Chukchi shelf and in the adjacent Canada Basin. When the pack-ice first retreats, open water phytoplankton blooms develop that utilize the nutrients (e.g. Hill and Cota, 2005). Furthermore, it has recently been determined that, earlier in the season, under-ice blooms can also form on the Chukchi shelf if enough sunlight is able to penetrate the first-year ice (Arrigo et al., 2014; Lowry et al., 2014). As the nutrients are drawn down during the spring and summer, the phytoplankton blooms deepen in the water column, dictated by the location of the nutricline – which in turn is largely determined by the presence of the winter water (Lowry et al., 2015).

The dense winter water is also of central importance for the maintenance of the halocline in the Canada Basin. After exiting the Chukchi shelf, much of the water is fluxed into the basin via turbulent processes. In particular, the two shelfbreak jets that transport the winter water along the edges of the Chukchi and Beaufort Seas are baroclinically unstable and spawn eddies that carry the water seaward (Pickart et al., 2005; Spall et al., 2008; von Appen and Pickart, 2012). Cold-core anti-cyclonic eddies populate the Canada Basin (Timmermans et al., 2008) and are the most commonly observed type of eddy in the western Arctic (Zhao et al., 2014). Their occurrence in the Canada Basin has been increasing in recent years (Zhao et al., 2016). As these features spin down they influence the stratification of the halocline, which is critical because this limits the vertical heat flux from the warm Atlantic layer below (that would otherwise melt the pack-ice). Recently it has been shown that a significant amount of the water exiting the Chukchi shelf forms a westward-flowing current along the continental slope of the Chukchi Sea (Corlett and Pickart, submitted). This may be another effective mechanism for transporting winter water into the basin.

Because of the overall dearth of observations in the Chukchi Sea during the cold months of the year, relatively little is known about the formation, modification, and circulation of winter water on the shelf. It is documented that such cold and dense water is formed in the northern Bering Sea (e.g. Muench et al., 1988) which then flows northward through Bering Strait from

roughly January through April (Woodgate et al., 2005). Hence there is a steady supply of winter water to the Chukchi Sea from the south, but presently the degree to which the water is altered as it progresses across the shelf is not well documented. Year-long mooring records from select areas on the shelf have demonstrated that the winter water can be further densified within large polynyas. In particular, re-freezing within the Northeast Chukchi Sea polynya can produce a very salty and dense product known as hypersaline winter water (Weingartner et al., 1998). It has also been shown that the degree of modification within this polynya varies from year to year (Itoh et al., 2012). However, it is currently unknown if modification of winter water takes place throughout the central Chukchi shelf, and if smaller leads (versus large polynyas) play a role in this.

The transport of Pacific water from Bering Strait through the Chukchi Sea occurs along three main pathways (Figure 1): via Hope Valley in the west (Weingartner et al., 1998), via the Central Channel (Weingartner et al., 2005), and via the Alaskan Coastal Current in the east (Paquette and Bourke, 1974). There is increasing evidence, however, that the flow is not nearly as rigidly set along these three distinct pathways as originally thought. In particular, it is now known that a portion of the western branch veers eastward to the north of Herald Shoal and joins the central branch (Pickart et al., 2010; Pickart et al., 2016). Also, as the water approaches Hanna Shoal it appears to split into two branches that progress around both sides of the shoal, subsequently dividing into even smaller filaments (Pickart et al., 2016). Sparsely placed moorings on the shelf have documented that winter water flows along the main pathways during winter and spring (e.g. Woodgate et al., 2005; Weingartner et al., 2005). Furthermore, hydrographic surveys have revealed that winter water is still present within the pathways on the northern portion of the shelf in the early summer (Pickart et al., 2016). However, the extent to which the cold water is present outside of these pathways – prior to summer – has yet to be determined.

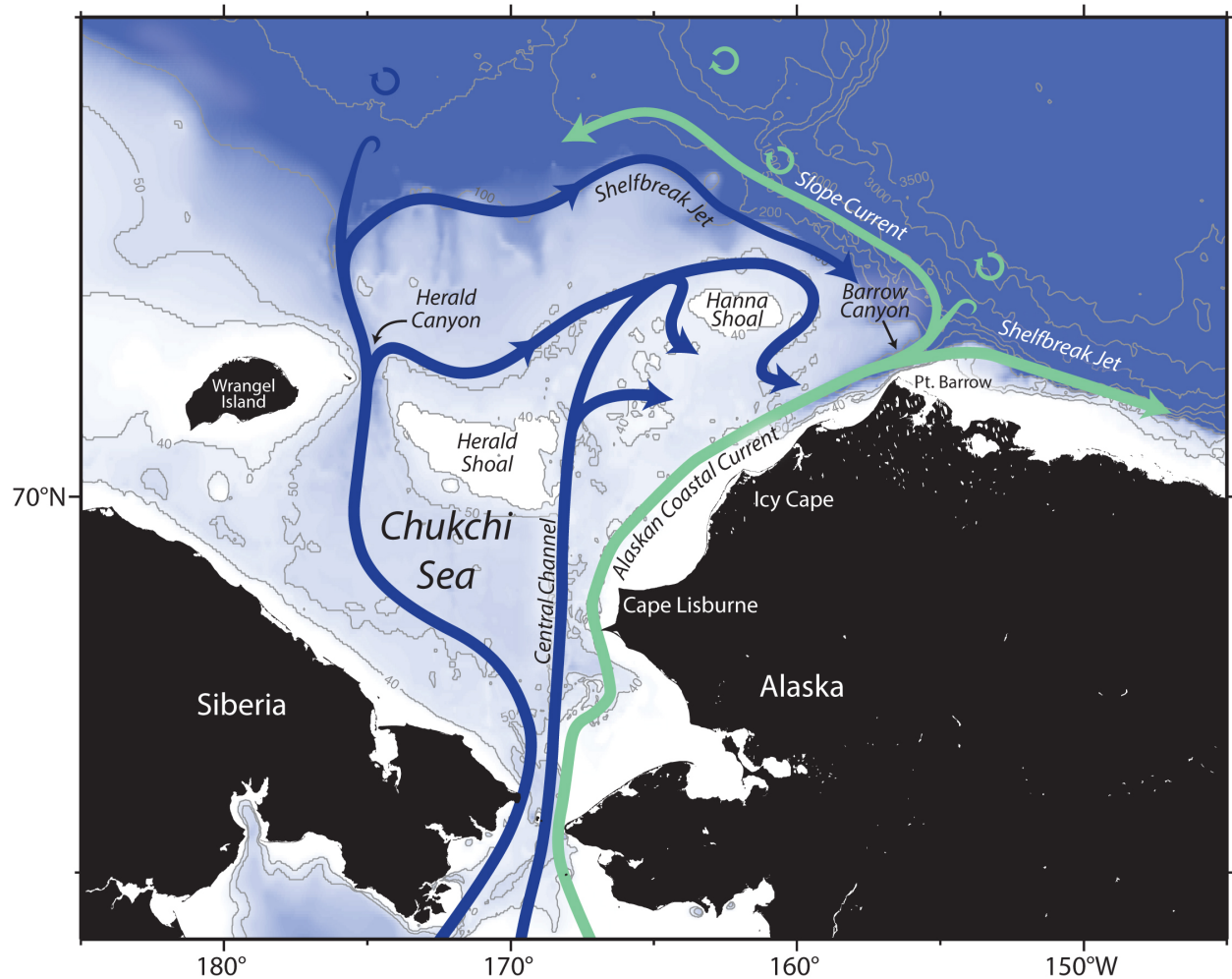


**Figure 1:** Schematic circulation of the Chukchi Sea (after Corlett and Pickart, submitted) and geographical place names.

In this study we use data from a springtime, broad-scale survey of the northeast Chukchi Sea to investigate the distribution and characteristics of winter water on the shelf. We demonstrate that winter water was prevalent throughout the study region—both within the main flow pathways and outside of them. The data reveal that the density structure of the shelf during this time of year can be characterized as a two-layer system, and we investigate various aspects of this. In addition, we assess the ability of the water column to be homogenized into a single layer via atmospheric forcing, which modifies the winter water by salinizing it through sea ice formation and brine rejection. The structure of the paper is as follows. We begin with a presentation of the data set followed by a general description of the hydrographic conditions on

the shelf. Next we examine characteristics of the surface mixed layer. Using a simple set of models, we investigate the ability of the atmospheric forcing to overturn the water column, creating a single layer. We then consider the modification of winter water in large polynyas versus smaller leads, which sheds light on how the entire Chukchi shelf could be filled with winter water at the end of the cold season. Lastly, we investigate the atmospheric conditions during the cruise and assess how representative they were for this time of year.

## **2. Data and methods**

In response to the discovery of massive under-ice blooms in the Chukchi Sea (Arrigo et al., 2014), a field program was carried out in late-spring 2014 entitled “The Study of Under Ice Blooms in the Chukchi Ecosystem” (SUBICE). This consisted of an interdisciplinary cruise with measurements of the physical, chemical, and biological state of the water column, sea ice, and benthos. The main goal of the SUBICE cruise was to sample pre-, during, and post-bloom conditions as a means to understand how and why these blooms occur and the physical drivers behind them. The present study focuses on the physical measurements collected during the field program.

### **2.1 Shipboard hydrographic and velocity data**

The shipboard hydrographic and velocity data used in the study were obtained during a 6-week cruise on the USCGC *Healy* (16 May – 20 June 2014). During this time, 251 water column stations were occupied comprising 15 transects (Figure 2). Due to difficult ice conditions, we were unable to sample the very northeast portion of the shelf, including Barrow Canyon. Also, in this study we do not consider any of the data south of Cape Lisburne. At each station a Sea-Bird 911+ conductivity-temperature-depth (CTD) system was mounted on a 12-position rosette with 30 liter bottles. The temperature sensors were calibrated at Sea-Bird before and after the cruise, and the accuracy was determined to be 0.001°C. Because the Chukchi shelf is so shallow, the bottle salinity samples were not effective for calibrating the conductivity sensors. As such, following previous studies (Pickart et al., 2010; Pisareva et al, 2015) we regressed the conductivity data from the two sensors against each other, which showed a tight relationship (after removing outliers). Based on this, the accuracy of the salinity measurements was deemed to be 0.008. Nutrients were measured from the water samples, typically at the following depths:

2, 5, 10, 25, 50, 75, and 100 m, including a sample at the fluorescence maximum and one just above the bottom. The nutrient analysis was done using a Seal Analytical continuous flow Auto-Analyzer 3, following a modification of the method used by Armstrong et al. (1967).

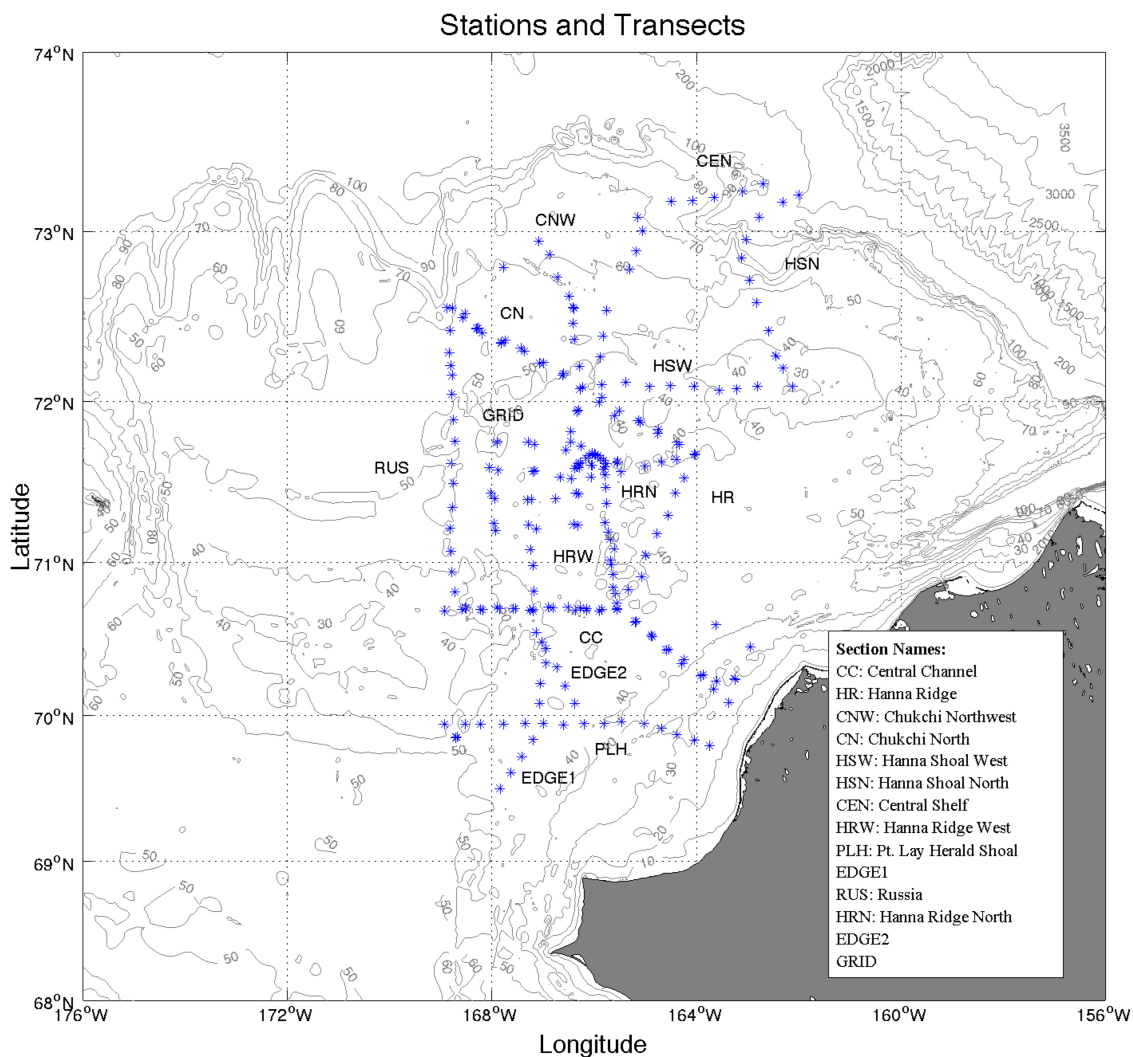


**Figure 2:** Locations of the hydrographic stations occupied on the 2014 cruise. See the legend for transect names. The Bering Strait line that was occupied is not considered in this study. The bathymetry is from IBCAO version 3.

Velocity of the water column was measured using *Healy's* vessel-mounted RDI Ocean Surveyor 150 kHz acoustic Doppler current profiler (ADCP). The vertical coverage of the ADCP extends from approximately 18 meters below the surface to approximately 10-15 meters above

the seafloor. Due to the extensive ice cover encountered during most of the cruise, velocity profiles were only obtained at the station sites (i.e. while the ship was not steaming). The reader is referred to Pickart et al. (2016) for a description of the processing procedure. After the velocities were calculated, the barotropic tidal signal was removed from each profile using the Oregon State University model <http://volkov.oce.orst.edu/tides> (Padman and Erofeeva, 2004).

As part of the analysis, vertical sections of hydrographic variables were constructed. This was done using a Laplacian-spline interpolation scheme with a typical grid spacing of 5 km in the horizontal and 2 m in the vertical for the CTD variables, and 10 km and 10 m, respectively, for nutrients. The variables considered are potential temperature referenced to the sea surface (hereafter referred to simply as temperature), salinity, potential density referenced to the sea surface (hereafter referred to as density), and nitrate. In addition, sections of absolute geostrophic velocity were made by referencing the thermal wind shear to the direct ADCP measurements following the procedure in Pickart et al. (2016).

Most of the CTD profiles on the shelf had a two-layer structure: a surface mixed layer separated from a bottom boundary layer by a sharp interface. A typical station is shown in Figure 3 (from the central part of the shelf). Using a Matlab Graphical User Interface (GUI), we determined various characteristics of the surface and bottom mixed layers. The vertical extent of each layer was determined following the technique used by Pickart et al. (2002). Specifically, each layer was initially identified visually using the GUI, then a two standard deviation envelope was plotted over these two regions (red lines in Figure 3). The final mixed layer depths were then taken to be the locations where the profile passed permanently outside of the envelopes. In the example shown in Figure 3, the surface mixed layer is slightly stratified in temperature, but is neutrally stable in both salinity and density. The bottom boundary layer displays a small degree of stratification, but this is within the precision of the conductivity sensor. For each mixed layer we determined a line of best fit (blue lines in Figure 3). We also tabulated the change in density between the surface and bottom mixed layers, which hereafter is referred to as the density jump.

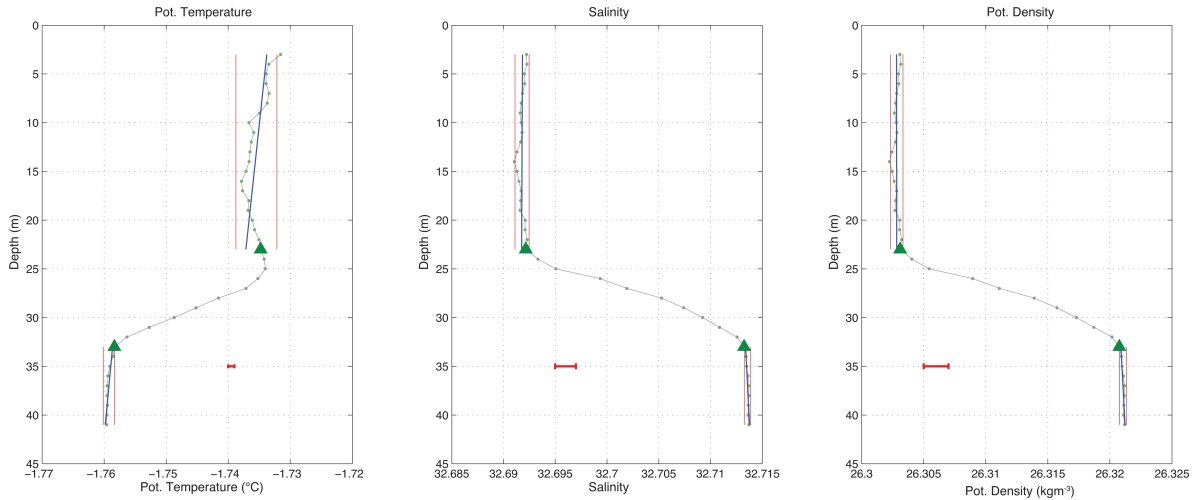


**Figure 3:** Vertical profiles of (a) potential temperature, (b) salinity, and (c) potential density for a typical CTD station containing newly ventilated winter water. The surface and bottom mixed layers are colored green. The red lines denote the two-standard deviation envelope used to identify the mixed layers, and the blue lines are the regression lines (see text). The green triangles mark the end points of the density interface between the two mixed layers. The red bars denote the precision of the CTD sensors.

## 2.2 Shipboard meteorological data

In order to compute turbulent air-sea heat fluxes, we used meteorological data obtained from the ship. Wind measurements were collected by four sensors: one acoustic anemometer on the bow mast, one on the starboard yard arm, and mechanical anemometers on the starboard and port yard arms (the yard arm is a horizontal pipe located above the ice pilot station). A comparison of these records, however, indicated that each of the sensors had problems during portions of the cruise. For the first two weeks, only the acoustic sensors collected valid data. Once all four sensors were on line, the bow mast unit frequently showed different wind speeds than the other three units. Since this typically occurred when the relative wind direction was from the stern, the discrepancies were likely caused by blockage from the ship's superstructure. Similarly, the starboard and port yard arm sensor readings suggested blockage when relative wind direction was from port and starboard, respectively. We therefore constructed a timeseries based on the yard arm sensors only, selecting the side with least blockage as indicated by the relative wind direction. When available, we used the data from the mechanical sensors since the

acoustic yard arm sensors showed occasional drops in absolute wind speed, even when blockage was minimal.

Using the record of wind speed so constructed, together with shipboard measurements of surface air temperature, surface humidity, and sea surface temperature, we computed timeseries of sensible and latent heat fluxes. This was done using the well-established COARE 3 bulk algorithm (Fairall et al., 2003). The data were sub-sampled to a 6 hourly time interval for the calculation. A comparison of *Healy's* meteorological records with comparable fields extracted from the Interim Reanalysis of the ECMWF-ERA-Interim (ERA-Interim) (Dee et al., 2011) along the ship track showed good agreement. In order to calculate the total heat flux, the net longwave radiative flux from the ERA-Interim was used. We note that ERA-Interim was among the best performing reanalyses in a comparison with Baseline Surface Radiation Network (BSRN) observations from Pt. Barrow, AK and Ny Alesund, Norway (Zib et al., 2012). Following Pickart et al. (2016), we neglect the net shortwave radiative flux so that the total heat flux is representative of conditions during the night, when much of the ice formation occurs in spring.

### **2.3 Atmospheric reanalysis fields**

To characterize the broad-scale atmospheric patterns impacting the Chukchi Sea we used the same ECMWF-ERA-Interim data set. The spatial and temporal resolution of ERA-Interim is 0.75 degrees and 6 hours, respectively. The dataset runs from 1979 to the present, and we consider the 36-year period 1979-2014 in order to put 2014 into historical context.

### **2.4 Satellite Ice data**

Our study uses Advanced Microwave Scanning Radiometer 2 (AMSR-2) data to characterize the sea ice concentration on the shelf over the winter and spring of 2014. AMSR-2 is a 6.25 km product with daily resolution. The data come from the Global Change Observation Mission 1<sup>st</sup>-Water satellite. It measures seven frequency bands from 6.925 GHz to 89.0 GHz (Beitsch et al, 2014). The data were downloaded from the University of Bremen ([http://www.iup.uni-bremen.de:8084/amsr2data/asi\\_daygrid\\_swath/n6250/2014/](http://www.iup.uni-bremen.de:8084/amsr2data/asi_daygrid_swath/n6250/2014/)).

## 2.5 Polynya model

As part of our analysis we use a polynya model to estimate the production of salt due to the formation of ice. The model is the same as that employed by Pickart et al. (2016). It is used here both in a stationary frame of reference and in a Lagrangian frame, following parcels being advected northwards through the Chukchi Sea. The model calculates sea ice production according to

$$P = \frac{Q_{net}}{\rho_{ice} L_h},$$

where  $Q_{net}$  represents the net cooling surface flux ( $\text{W}/\text{m}^2$ ),  $\rho_{ice}$  represents the density of sea ice ( $\text{kg}/\text{m}^3$ ),  $L_h$  represents the latent heat of fusion ( $\text{J}/\text{kg}$ ) (Cavalieri and Martin, 1994), and  $P$  represents the rate at which ice is produced ( $\text{kg}/\text{s}$ ).

The salinity of the new ice,  $S_i$ , is

$$S_i = 0.31S_w,$$

where  $S_w$  represents the salinity of the surface water. The model combines these two equations to obtain the salt flux according to

$$F_s = \rho_{ice} P (S_w - S_i),$$

where  $F_s$  represents the salt flux generated by ice formation (Cavalieri and Martin, 1994).

In the stationary reference case (section 4.2), the salt flux is calculated at a time step of 10 minutes. This is subsequently used as input to a one dimensional mixing model (see below) to investigate convective overturning of the water column, where CTD profiles from the cruise are used as initial conditions. In the Lagrangian case (section 4.3), the salt flux is calculated daily following water parcels, with the assumption that the surface water is at the freezing point. Polynya conditions are assumed to occur when the ice concentration is less than 80%. The salt produced is assumed to mix throughout the water column, and the resulting change in salinity following the parcel is tabulated. The reader is referred to Pickart et al. (2016) for details of the Lagrangian application of the model.

## **2.6 One-dimensional mixing model**

To investigate the ability of the water column to overturn due to brine rejection during ice formation, we employ the one-dimensional mixing model of Price et al. (1986), hereafter referred to as the PWP model. The model is driven by the negative freshwater flux calculated using the polynya model described above for the stationary reference case, using CTD profiles from the cruise as initial conditions. Both the heat flux and the momentum flux are assumed to be zero. The vertical resolution used for the PWP model is 1 m, and we run it with a time step of 10 min. All of the initial CTD profiles have a surface mixed layer, and the model is used to document the deepening of the layer due to the negative freshwater flux from the surface.

## **3. Hydrographic setting**

### **3.1 Water mass distribution**

A variety of water masses are found on the Chukchi shelf throughout the course of the year. The cold winter water near the freezing point that flows northward through Bering Strait from approximately January through April (Woodgate et al., 2005) is referred to as newly ventilated winter water (NVWW). As this water warms later in the season, either via solar heating or mixing with summer water masses on the shelf, it becomes remnant winter water (RWW). RWW constitutes the cold halocline layer in the Canada Basin (e.g. Steele et al., 2004). In addition to these two winter water masses, there are two types of Pacific-origin summer waters that are found seasonally on the Chukchi shelf. Bering summer water (BSW) is a combination of Anadyr water and central Bering shelf water that mix with each other north of Bering Strait on the southern portion of the shelf (e.g. Pisareva et al., 2015). This water mass has also been referred to as western Chukchi summer water (Shimada et al., 2001), summer Bering Sea water (Steele et al., 2004), and Chukchi summer water (von Appen and Pickart, 2012). The second Pacific-origin summer water is the Alaskan coastal water (ACW), which is warmer, fresher, and more strongly stratified than BSW. It enters the Chukchi Sea via the Alaskan Coastal Current.

The final three water masses found in the Chukchi Sea are meltwater (MW), Atlantic water (AW), and Siberian coastal water (SCW). The former has two varieties (e.g. Gong and Pickart, 2015): early-season MW which is near the freezing point, and late-season MW which

has been warmed by solar heating. AW is transported eastward along the continental slope of the Chukchi Sea by the Arctic-wide cyclonic boundary current system (Aagaard, 1984; Rudels et al., 2004; Karcher et al., 2007; Aksenov et al., 2011). Periodically this warm and salty water is upwelled into Barrow Canyon in the east (e.g. Aagaard and Roach, 1990; Pisareva et al., this issue) and Herald Canyon in the west (Pickart et al., 2010). Under certain circumstances the AW can penetrate far onto the shelf (Bourke and Paquette, 1976; Ladd et al., 2016). The SCW originates as runoff from the Siberian coast and is found predominantly in the Siberian Coastal Current which flows towards Bering Strait (e.g. Weingartner et al., 1999). At times this water mass can be found in Herald Canyon and also on the central shelf (Pisareva et al., 2015).

A typical summertime survey of the Chukchi Sea will measure many (if not all) of these water masses (e.g. Gong and Pickart, 2015; Pisareva et al., 2015). During our late-spring survey, however, the majority of the water on the northeast Chukchi shelf was NVWW (Figure 4a). Here we define NVWW as colder than  $-1.6^{\circ}\text{C}$  and saltier than 31.5. This definition is consistent with past studies (e.g. Itoh et al, 2015; Gong and Pickart, 2015; Pickart et al., 2016). As noted in the introduction, NVWW can be further transformed within the Northeast Chukchi Sea polynya to form a very salty water mass known as hypersaline winter water. Weingartner et al. (1998) defined two classes of this salty water – one with salinities between 33 and 33.6, and the other with salinities  $> 34$ . As seen in Figure 4a, neither of these hypersaline classes were observed during the SUBICE cruise (keep in mind that we were unable to sample the very northeast part of the shelf (Figure 2)). Excluding the stations seaward of the shelfbreak (and the Bering Strait transect occupied at the start of the cruise), more than 96% of the water measured during the cruise was NVWW (Fig. 4a).

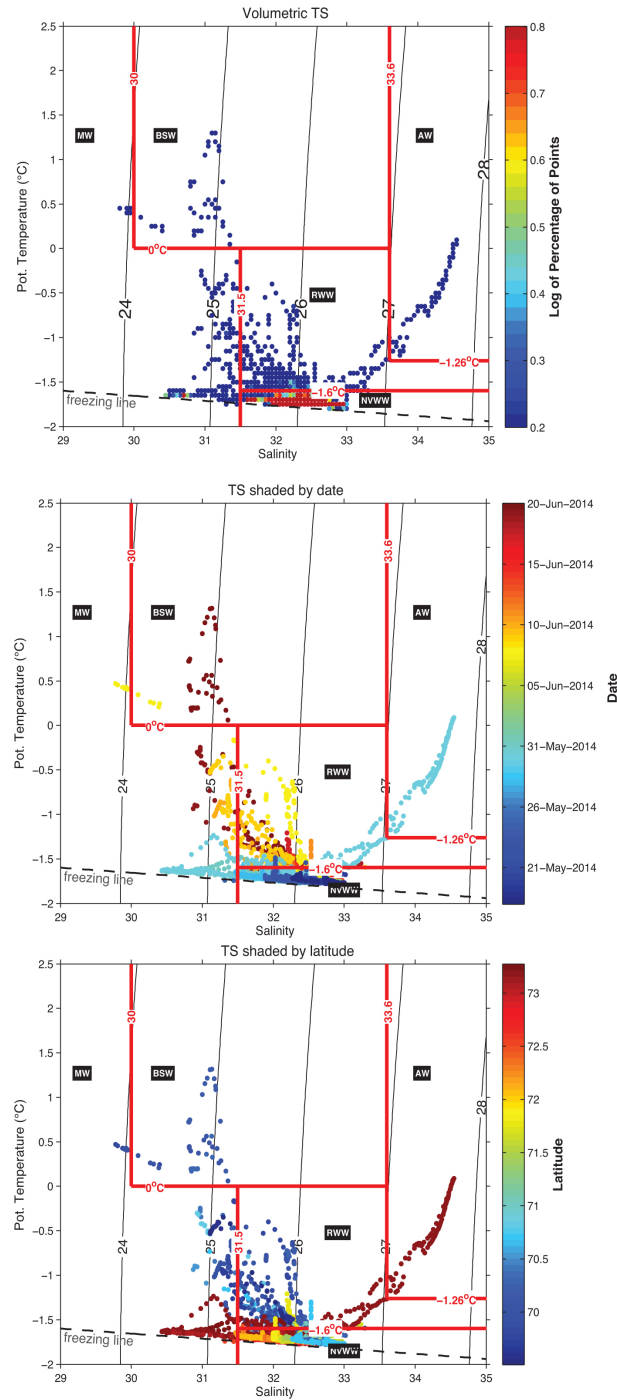


**Figure 4:** (a) Volumetric T/S diagram for the all the stations occupied north of 68°N during the cruise. The color denotes the number of points within bins of 0.05°C in temperature by 0.05 in salinity. The water mass boundaries are denoted by the red lines. The freezing line is indicated. The water masses are: NVWW = newly ventilated winter water; RWW = remnant winter water; BSW = Bering summer water; MW = meltwater; and AW = Atlantic water. (b) The same T/S diagram except that the points have been colored by date of occupation. (c) Same as (b) except the points have been colored by latitude.

To shed light on the space/time patterns of the different water masses sampled on the cruise, we constructed temperature-salinity (T/S) plots based on time (Figure 4b) and latitude (Figure 4c). Clear patterns emerged. The coldest NVWW (i.e. near the freezing point) was sampled early in the cruise (in late-May, Figure 4b). Not surprisingly, most of the RWW was measured in June, i.e. after the coldest winter water started to moderate. Nearly all of the BSW was measured at the very end of the cruise, at which time the leading front of the Pacific-origin summer water was entering the domain. There is also a clear division between the early-season MW and late-season MW. Geographically, one sees that all of the AW was located at the northern end of the domain, in particular, seaward of the shelfbreak (Figure 4c). Interestingly, this is also where we sampled the early-season MW, suggesting that signs of meltback were occurring off of the shelf. The late-season MW was observed in the southern part of the domain in the vicinity of the retreating ice edge. Consistent with the timing noted above, the BSW was confined to the southern end of the study region. Similarly, most of the RWW was found in this region as well. Finally, note that the NVWW was observed throughout the range of latitudes sampled on the cruise.

### **3.2 Water column structure**

Vertical sections were constructed for each of the 15 transects occupied during the cruise. Here we show three of the transects in order to point out some of the features that were unique to this late-spring survey (Figure 5). The first section extends across the Central Channel towards the Alaska coast (referred to as the CC line in Figure 2). This was the first transect sampled on the Chukchi shelf (north of Bering Strait), from 18-20 May. Strikingly, the entire section consisted of NVWW. Previous early-summer hydrographic surveys showed that this cold water mass was confined to the major flow pathways (Pickart et al., 2016). Clearly this is not the case earlier in the season. The saltiest winter water was found in the Central Channel (Figure 5a), but the coldest winter water was found on the eastern portion of the transect. (Note: this is not evident from the temperature color bar in Figure 5; we have chosen this color bar to be consistent with numerous previous studies.) The section of absolute geostrophic velocity reveals the Central Channel flow branch, which exceeds  $15 \text{ cm s}^{-1}$  on the eastern side of the channel. While there is

NVWW everywhere in the section, the saltiest (and therefore densest) winter water is confined to the major flow path passing through the channel.

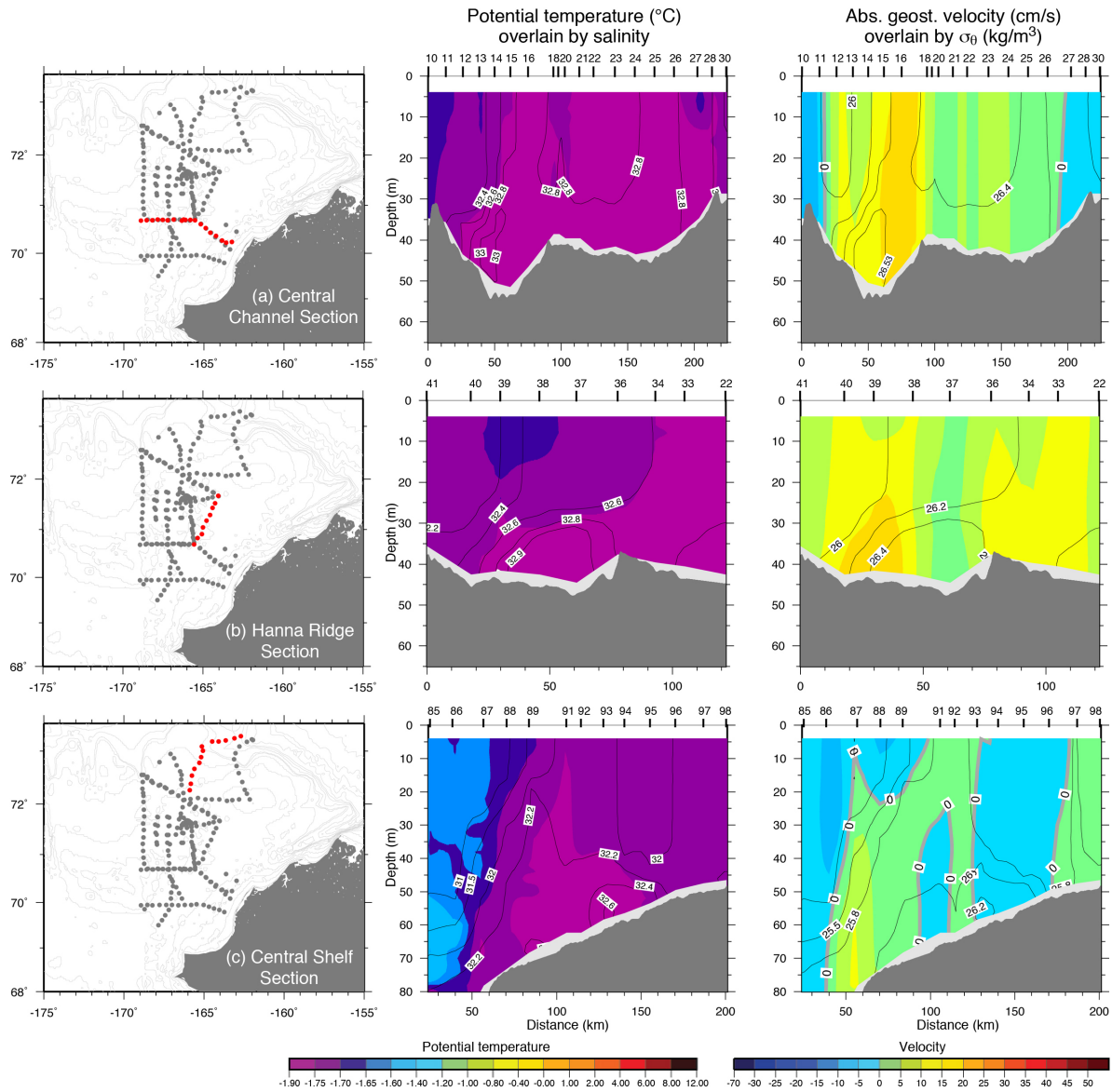


**Figure 5:** Vertical sections of potential temperature (color) overlain by salinity (contours), and absolute geostrophic velocity (color) overlain by potential density (contours). Positive velocities are into the page, flowing northward. The bathymetry is from the ship’s echosounder. Station numbers are listed along the top. (a) The Central Channel section; (b) the Hanna Ridge section; (c) the central shelf section. The left-hand panel in each row shows the location of the transect (red-colored stations).

The next transect we consider is the Hanna Ridge line (section HR in Figure 2), which was occupied 22-23 May (shortly after the CC section). This was positioned along a portion of the corrugated ridge between Herald and Hanna shoals (the biggest gap in the ridge is of course the Central Channel; see the bathymetry in Figure 2). As with the CC line, this section contained exclusively NVWW (Figure 5b). The notable aspect of this transect is that the small bathymetric depression (between stations 36 and 40) contains the saltiest and densest water. Furthermore, the northern side of this dense feature is associated with a bottom-intensified geostrophic current to the east. Together with nearby data (see section 3.5 below), this implies that NVWW is “leaking” from the main Central Channel flow pathway to the east through gaps in the ridge. As was the case with the CC section, the saltiest winter water is embedded within a region of enhanced flow, suggesting that, while NVWW is prevalent everywhere, the currents on the shelf advect the densest variety of this water mass.

The final section we present is the CEN line, which extends from the upper continental slope to the outer portion of the shelf (Figure 2). This was one of the two sections that crossed the shelfbreak, and it reveals that the NVWW was confined to the Chukchi shelf. Seaward of the shelfbreak the dominant water mass in the basin was RWW, which was clearly more than a year old (i.e. ventilated on the Chukchi shelf during a previous winter). This water appears in the T/S plots shown above as the only RWW that was sampled both early in the cruise (Figure 4b) and at a northern latitude (Figure 4c). On the shelf there is nothing but NVWW, some of it very weakly stratified (station 96 had a neutrally stable density profile from top to bottom). The density front at the edge of the shelf between the NVWW and RWW supports a bottom-intensified, eastward-flowing shelfbreak jet, which has been observed previously (e.g. Mathis et al., 2007; Pickart et al., 2016; Corlett and Pickart, submitted).

### **3.3 Lateral Patterns**

The volumetric T/S diagram (Figure 4a), together with the vertical sections, indicate that most of the domain sampled during the SUBICE cruise contained NVWW. To assess if there were any spatial patterns, we constructed lateral maps. As mentioned above, previous early-

summer surveys measured NVWW only within the main flow pathways and it was mainly restricted to the lower part of the water column. To highlight the difference in the hydrographic nature of the shelf during the late-spring time period, we averaged the properties at each of the stations in the upper 25 m of the water column (which for the previous surveys would show very little, if any, winter water). The resulting distribution of average temperature reveals that NVWW occupied the surface layer over most of the measurement domain (Figure 6a). The main exceptions were the region seaward of the shelfbreak and the southern portion of the study area, which was sampled at the end of the cruise. Much of the region south of the CC line was in open water at that point, and the warm temperatures are indicative of RWW (with some BSW and late-season MW near the surface). Recall that NVWW is defined as water colder than  $-1.6^{\circ}\text{C}$ . Hence, there was spatial variation in the temperature of this water mass (the coldest NVWW sampled on the cruise was  $-1.78^{\circ}\text{C}$ ). While there is no obvious pattern in Figure 6a, the T/S diagrams of Figures 4b,c reveal that, early in the cruise, the NVWW was a bit warmer and fresher to the north (progressing along the freezing line).

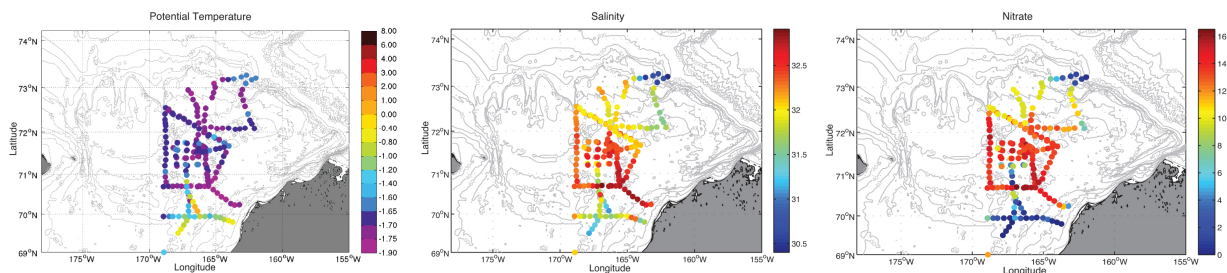


**Figure 6:** Lateral property plots. (a) Potential temperature ( $^{\circ}\text{C}$ ) averaged over the top 25 m of the water column. The bathymetry is from IBCAO version 3; (b) Same as (a) except for salinity; (c) Same as (a) except for nitrate ( $\mu\text{M l}^{-1}$ ).

As was true for the temperature, the salinity values on the continental slope were distinct from the outer shelf; in particular, the basin water was markedly fresher (Figure 6b). Also in line with the temperature, the water sampled late in the cruise in the southern part of the domain was noticeably different in salinity compared to waters farther north (again fresher, but not as fresh as the basin water). However, in contrast to the temperature, there is a clear lateral trend in the salinity of the NVWW on the shelf. In particular, north of about  $72^{\circ}\text{N}$  the winter water becomes fresher by about 0.3. Furthermore, there is a zonal gradient in the salinity of the NVWW, with fresher values closer to Hanna Shoal. This same trend in NVWW salinity was found by Pickart

et al. (2016) using early summertime data, except in that case the average was done for the deep part of the water column (where the NVWW was found). We investigate this lateral salinity trend further in section 4.3.

As noted in the introduction, the NVWW is critically important to the regional ecosystem because of its high nutrient content, which spurs primary production (Hill and Cota, 2005; Lowry et al., 2015; Pickart et al., 2016). Our SUBICE cruise revealed that, in late-spring, the nitrate levels in the upper part of the water column are generally quite high (see also Arrigo et al., submitted). Figure 6c shows the average value over the top 25 m (the distribution is nearly identical if only the near-surface values are plotted). The water seaward of the shelf is low in nitrate since, as noted above, it is RWW that is at least a year old. In the southern part of the domain the levels are low because the nitrate has been drawn down due to bloom activity in the nearly open water encountered late in the cruise. Another region of low nitrate was found on the eastern end of the CC line (near Icy Cape). As seen in Figure 5a, this region contained NVWW, yet the nitrate concentration in the upper 25 m was fairly low. During the occupation of the eastern portion of this line the winds were northerly and the flow near the coast was to the south. This suggests that coastal upwelling was taking place, which might have influenced the nitrate distribution.

Notably, in the central portion of our study domain – where the NVWW was located – the lateral distribution of nitrate shows a similar pattern to that of the salinity (compare Figures 6b and c). In particular, the nitrate concentrations in the upper water column are significantly lower north of 72°N. Regressing nitrate against salinity (excluding the continental slope stations and the sections occupied at the end of the cruise) this reveals a statistically significant relationship, with saltier NVWW generally higher in nitrate (see also Arrigo et al., submitted). The likely reasons for this are explored in section 4.

### **3.4 Temporal evolution**

During the cruise we occupied the CC section (across the Central Channel, Figure 2) in mid-May (early in the cruise) and again in early-June. In addition, the section was occupied in late-June in 2010 during a previous field program (Pickart et al., 2016). This provides the opportunity to look at the evolution of the water column at this location during the spring to summer transition. We consider the hydrography, velocity, and nitrate concentration (Figure 7).

The first occupation was discussed previously, but in Figure 7 (top row) it is now evident that the saltiest NVWW in the Central Channel pathway was also the highest in nitrate. We hasten to add, however, that the nitrate concentrations were high throughout the section with very little vertical structure. The only exception was near the coast in the reversed flow.

Three weeks later the conditions had changed considerably (Figure 7, middle row). Warmer, fresher water (but still within the T/S range of NVWW) was present in the upper 20 m of the water column in the Central Channel, presumably advected there via the middle flow pathway (see Figure 1). This pathway is again evident in the section of absolute geostrophic velocity. One sees that the nitrate in this region is largely drawn down, which likely took place upstream in near-open water (the ice cover over the Central Channel during the second occupation was still > 90%). Low nutrient concentrations were also found at the eastern end of the section in the region of reversed flow, as was the case in the earlier occupation. Unlike the first transect, however, the (much lower) nutrient values in early-June near the coast were likely due to local draw down. This is consistent with the reduced ice cover there (30% versus 100% during the first crossing in mid-May), which also can explain the presence of RWW near the coast due to local solar heating. The last feature of note in the second occupation is the high nutrient signal at stations 122-123. This is associated with salty NVWW embedded within a region of enhanced northward flow. Hence, while the Central Channel pathway was advecting dense, nitrate-enriched winter water northward in the first crossing, the same was true of the coastal pathway in the second crossing.

The transect in late-June (occupied in 2010) showed a vastly different situation. The upper half of the water column was filled with warm BSW, separated by a halocline from winter water near the bottom (Figure 7, bottom row). There were three “pockets” of NVWW: one in the Central Channel pathway, one in the coastal pathway, and one within a region of weak southward flow between the two pathways. As discussed in Pickart et al. (2016), these were the last vestiges of NVWW flowing through the Chukchi Sea. Each of the three regions of NVWW was associated with enhanced nitrate, while the nitrate levels in the BSW were generally low due to consumption by open water blooms. The highest levels of chlorophyll were found at the interface between the NVWW and BSW (not shown), emphasizing the importance of the NVWW in driving primary production, even at depth (see Lowry et al. (2015) for details).

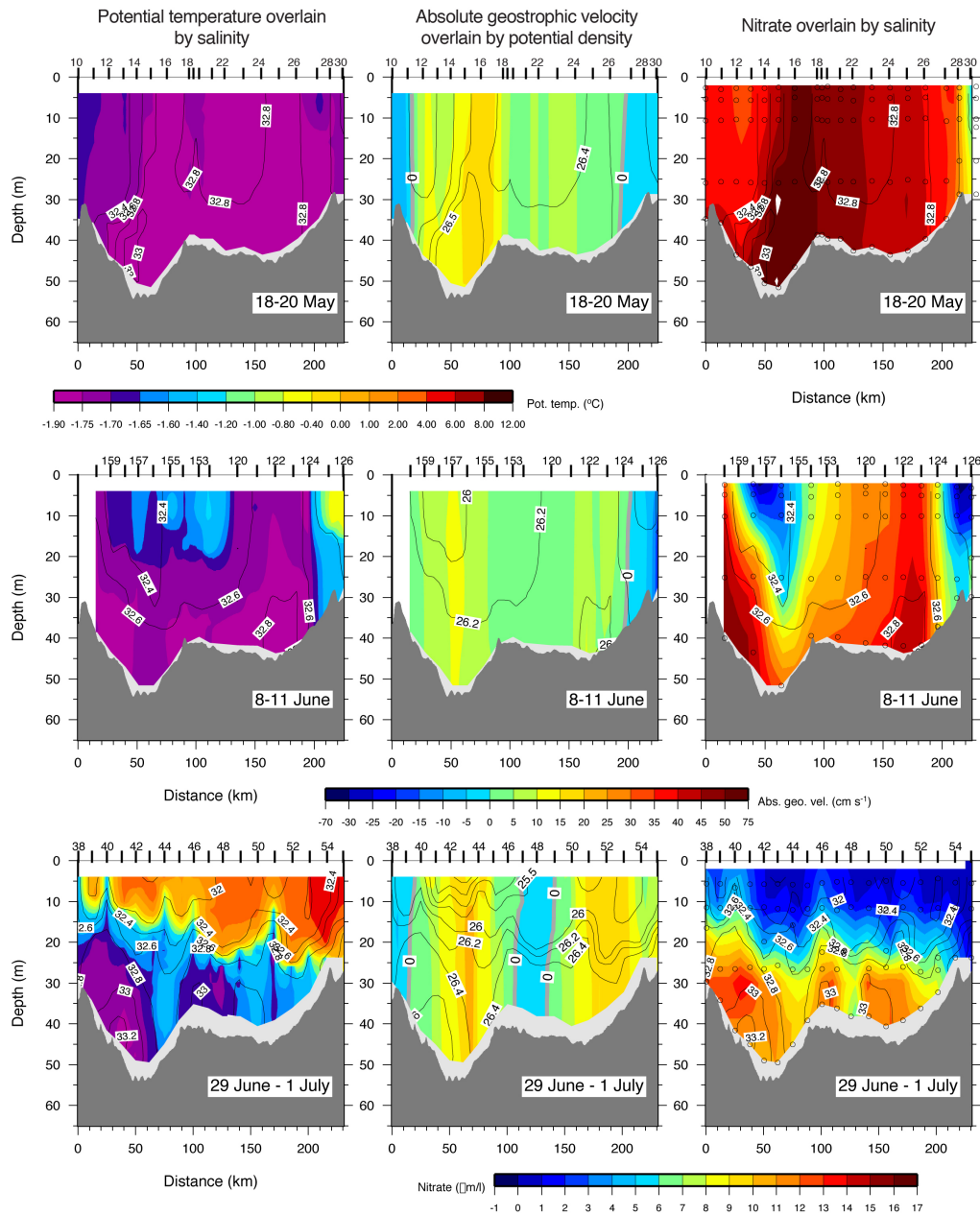


**Figure 7:** Repeat occupations of the Central Channel section (section CC in Figure 2). Top row: 18-20 May, 2014; middle row: 8-11 June, 2014; bottom row: 29 June – 1 July, 2010. The left-hand column shows sections of potential temperature (color, °C) overlain by salinity (contours). The middle column shows sections of absolute geostrophic velocity (color,  $\text{cm s}^{-1}$ ) overlain by potential density (contours,  $\text{kg m}^{-3}$ ). The right-hand column shows sections of nitrate (color,  $\mu\text{M l}^{-1}$ ) overlain by salinity (contours), where the circles denote the water sample locations. Station numbers are listed along the top of each plot.

### 3.5 Velocity field

In the repeat occupations of the CC transect presented in the previous section, one sees that both the Central Channel pathway and the coastal pathway were present in each of the three realizations (the flow was clearly strongest in the 2010 occupation). Using data primarily from an early-summer survey of the Chukchi Sea in 2011, Pickart et al. (2016) constructed an updated circulation scheme for the northeast Chukchi shelf, which is depicted schematically in Figure 1 (see Figure 9 of Pickart et al. (2016) for details). The new features presented in that study were: (1) the flow approaching Hanna Shoal bifurcates and flows around each side of the shoal; (2) a portion of the western flow branch diverts eastward on the north side of Herald Shoal and joins the central branch; and (3) some of the flow from the central branch “leaks” through the corrugated ridge between Herald and Hanna Shoals and progresses towards Barrow Canyon. It is of interest to know if our SUBICE survey indicates similar features.

In Figure 8 we present the depth-integrated ADCP flow vectors from our survey. The vectors that exceed  $10 \text{ cm s}^{-1}$  are colored red, which reveals the major flow paths (the red-shaded arrows are simply meant as a guide to the reader). Overall, the flow field measured in late-spring 2014 was remarkably consistent with that measured in early-summer 2011. In particular, the Central Channel pathway is evident, and one sees that the flow divides around the northern and southern sides of Hanna Shoal. There is also a signature of the coastal pathway (see also the vertical sections of absolute geostrophic velocity in Figure 7). Interestingly, one gets the impression that the coastal pathway bifurcates from the Central Channel pathway between  $70\text{-}70.5^\circ\text{N}$ . This is entirely feasible, since at this time of year the coastal pathway is not the Alaskan Coastal Current (which develops later in the season).

SUBICE mean ADCP vectors at CTD stations

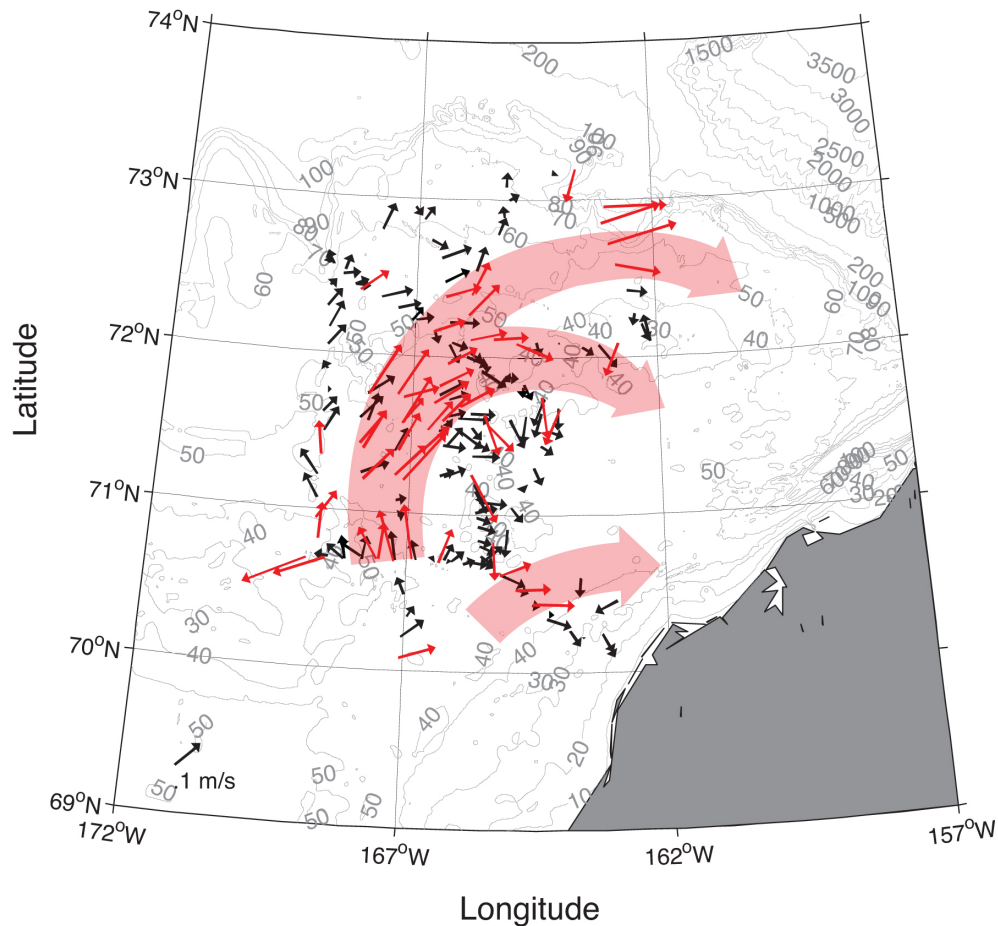


**Figure 8:** Depth-integrated velocity vectors from the shipboard ADCP. The vectors with magnitude  $> 10 \text{ cm s}^{-1}$  are colored red. The transparent red arrows are meant as guide to show the main flow pathways on the shelf.

Outside of the main pathways, the flow field in Figure 8 is also in line with the updated circulation scheme in Pickart et al. (2016). Clearly, a significant amount of flow progresses eastward through the corrugated ridge between Herald and Hanna Shoals. One particular example of this was shown above for the HR section (Figure 5b), but it seems to happen all along the ridge to varying degrees. The notion that part of the western pathway joins the central pathway is also supported by the SUBICE measurements (note the flow to the northeast between  $72\text{--}72.5^\circ\text{N}$  in the northwest part of the study domain). Finally, the flow along the upper continental slope is an expression of the Chukchi shelfbreak jet (see also Corlett and Pickart

(submitted)). The consistency of the flow field presented here with that of Pickart et al. (2016) suggests that these various features are permanent aspects of the circulation of Pacific-origin water on the Chukchi shelf – at least in spring and summer.

#### **4. Mixed layers**

As discussed above, the majority of the CTD profiles occupied during the survey displayed a two-layer structure, with a surface mixed-layer and bottom boundary layer separated by a sharp density interface (see Figure 3 for a typical example). Out of the 181 CTD stations taken on the shelf that contained NVWW, 176 had top mixed layers, 157 had bottom mixed layers, and 155 had both. Here we focus primarily on the height of the surface and bottom mixed layers and the strength of the density jump between them.

##### **4.1 Bottom boundary layers**

There were no obvious geographical or temporal trends in bottom boundary layer height across our survey domain. Previous theory (Trowbridge and Lentz, 1991; Lentz and Trowbridge, 1991) has demonstrated that, for flow over a sloping bottom, the size of the bottom mixed layer is sensitive to whether the interior flow (i.e. that above the layer) is upwelling-favorable or downwelling-favorable. In the former case – when the current is flowing with shallow water on the left – the upslope bottom Ekman layer flow tends to advect denser water beneath light water. This enhances the stratification and keeps the bottom layer small. In the latter case – when the current is flowing with shallow water on the right – the downslope Ekman flow brings light water beneath dense water which results in a statically unstable condition. The resulting convective adjustment causes the bottom mixed layer to increase in size. In the upwelling-favorable scenario the bottom boundary layers will reach a threshold maximum height, above which they will no longer grow. By contrast, in the downwelling scenario there is no such impediment on how thick the layer can be.

In an effort to determine if our data are consistent with this theory, we examined the conditions associated with each station and determined if it was an upwelling-favorable case, a downwelling-favorable case, or neither. This entailed considering the ADCP velocity data at the station and the slope of the local bathymetry. In order to get the most accurate estimate of the bottom slope we used the ship's echosounder data, which was corrected for variations in sound

speed and smoothed slightly to remove scatter. (We note that the digital databases are not sufficient in terms of resolution or accuracy for this calculation.) This bathymetric data meant that we could only consider stations where the ADCP velocity vector was approximately perpendicular to the transect. We also excluded stations that had weak bottom slopes (magnitudes  $< 10^{-4}$ ), which removed a large number of sites from consideration (keep in mind that much of the Chukchi shelf is relatively flat, particularly the part that we sampled). Even after applying these criteria we detected no systematic differences in the character of the bottom boundary heights for the upwelling- versus downwelling-favorable stations. In particular, there were no trends with respect to bottom slope, and the scatter in layer heights was similar in both cases. As shown below, we believe that this was because active convection was taking place during the first part of the cruise, which would hinder the applicability of the above theory to our observations.

#### **4.2 Surface mixed layers and convective overturning**

The average surface mixed layer height over the study domain was  $19.8 \pm 10.0$  m, and there were no distinguishable trends in space or time. However, one striking aspect of our data set was that the density jump between the surface layer and the bottom layer was typically very small. This in turn suggests that it would not take much surface buoyancy loss, and resulting convective activity, to erode this interface and homogenize the entire water column. In fact, 7 stations sampled during the cruise had a density jump of  $< 0.01 \text{ kg m}^{-3}$ . As noted earlier, previous studies using moorings on the Chukchi shelf have documented salinification of the near-bottom water within polynyas (Weingartner et al., 1998; Itoh et al., 2012). The open water quickly freezes and rejects brine into the surface water, which destabilizes the water column. This results in convective overturning, transporting the extra salt to depth. The deep mooring records indicate that the overturning can reach the bottom.

None of the stations in our survey were occupied in the Northeast Chukchi Polynya. Also, the satellite data indicate that, until the end of the cruise when meltback was occurring in the southern part of the domain, the ice cover was typically between 80-100%. This raises the question, does transformation of the NVWW occur away from large polynyas within smaller leads and openings? We note that there were many such small leads present in our study area, and most of the CTD stations occupied during the cruise were done in such openings

(operationally this was far easier than making a hole in the pack-ice using the ship). Furthermore, in a large number of instances these leads were actively re-freezing. We now assess the likelihood that modification of winter water takes place broadly across the Chukchi shelf within the concentrated pack ice. Specifically, we seek to determine how readily the CTD profiles measured during our cruise might be homogenized via convective overturning in re-freezing leads; that is, how quickly can the density jump between the surface and bottom mixed layers be eroded. Our approach is to use a polynya model with a realistic air-sea heat loss to compute the salt flux to the surface layer during ice formation. This flux is subsequently used to drive a one-dimensional mixed layer model with each CTD cast as an initial condition. The time it takes the water column to overturn is then tabulated for each site. While this should be considered a thought experiment, we argue that, based on the conditions noted above, it is likely that such overturning was happening during the cruise.

As explained in section 2.2, we used the shipboard meteorological data to construct a timeseries of turbulent heat flux and the ERAI radiative fields to estimate the longwave heat flux. These two timeseries are shown in Figure 9, along with the total heat flux. One sees that the total flux was positive (i.e. heat loss from the ocean) until early June, at which point there was an abrupt reduction. After this, the flux stayed fairly close to zero for the remainder of the sampling period. During the first two weeks of the cruise (18 May to 2 June), the average heat loss was  $\sim 150 \text{ W m}^{-2}$ . We use this value to force the polynya model.

The polynya model, described in section 2.4, assumes that the surface water is at the freezing point, and, as the ice forms, it is continually advected out of the region by the wind (i.e. the same wind that opened up the ice in the first place). Before running the model, we first estimated how much time it would take for the temperature of the surface water for each cast to be lowered to the freezing point when subject to the air-sea heat loss (this was done using the one-dimensional mixed layer model with no salt flux). Since these values were negligibly short, each CTD cast was taken to be at the freezing point. We then used the polynya model to calculate the negative freshwater flux due to ice formation at each site. Finally, this salt flux was used to force the PWP model as outlined in section 2.5.

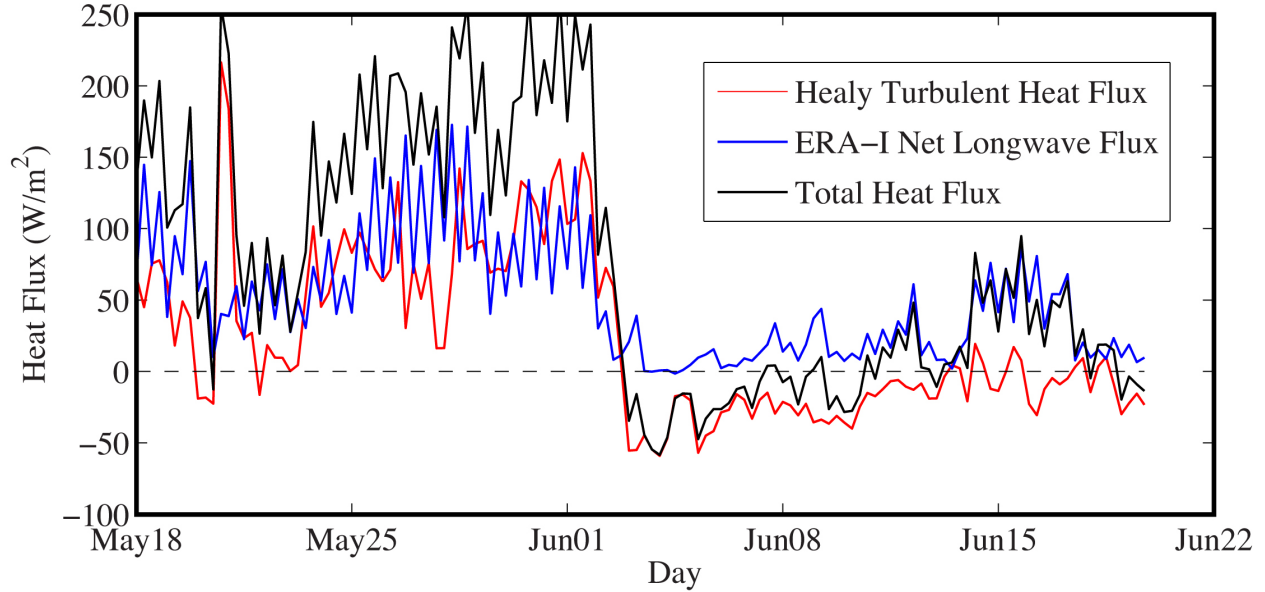


**Figure 9:** Timeseries of turbulent, longwave, and total heat flux at the location of the ship during the cruise.

We ran the combined polynya-PWP model for each of the CTD casts on the shelf that contained NVWW (181 stations). The mean overturn time was  $8.6 \pm 7.0$  hours. The minimum was only 20 minutes, and all but 4 stations overturned in less than 24 hours. These results imply that most of the profiles on the Chukchi shelf measured during the SUBICE cruise were poised for rapid overturning, particularly when subject to the heat fluxes experienced during the latter half of May. This also provides an explanation as to why we measured a number of profiles that were neutrally stable (or nearly so).

It is of interest to understand what factors influence the overturn time. As seen in Figure 10, there is a clear correlation between the size of the density jump between the two layers and the overturn time (using  $150 \text{ W m}^{-2}$  for all the stations). This correlation makes sense: the larger the density jump, the harder it is to erode the interface and bring the top mixed layer to the density of the bottom mixed layer. However, as is evident from the figure, for larger values of the density jump, there is more scatter in how long the water column takes to overturn. To explain this, we considered the thickness of the top mixed layer, which is indicated by color in Figure 10. One sees that, for a given density jump, the thicker the layer the longer it takes to overturn the water column. This is again reasonable, as the effect of a given salinity increase from brine rejection will be smaller if the mixed-layer is larger, since the brine must mix with more water and will therefore increase the overall density of the top mixed layer less.

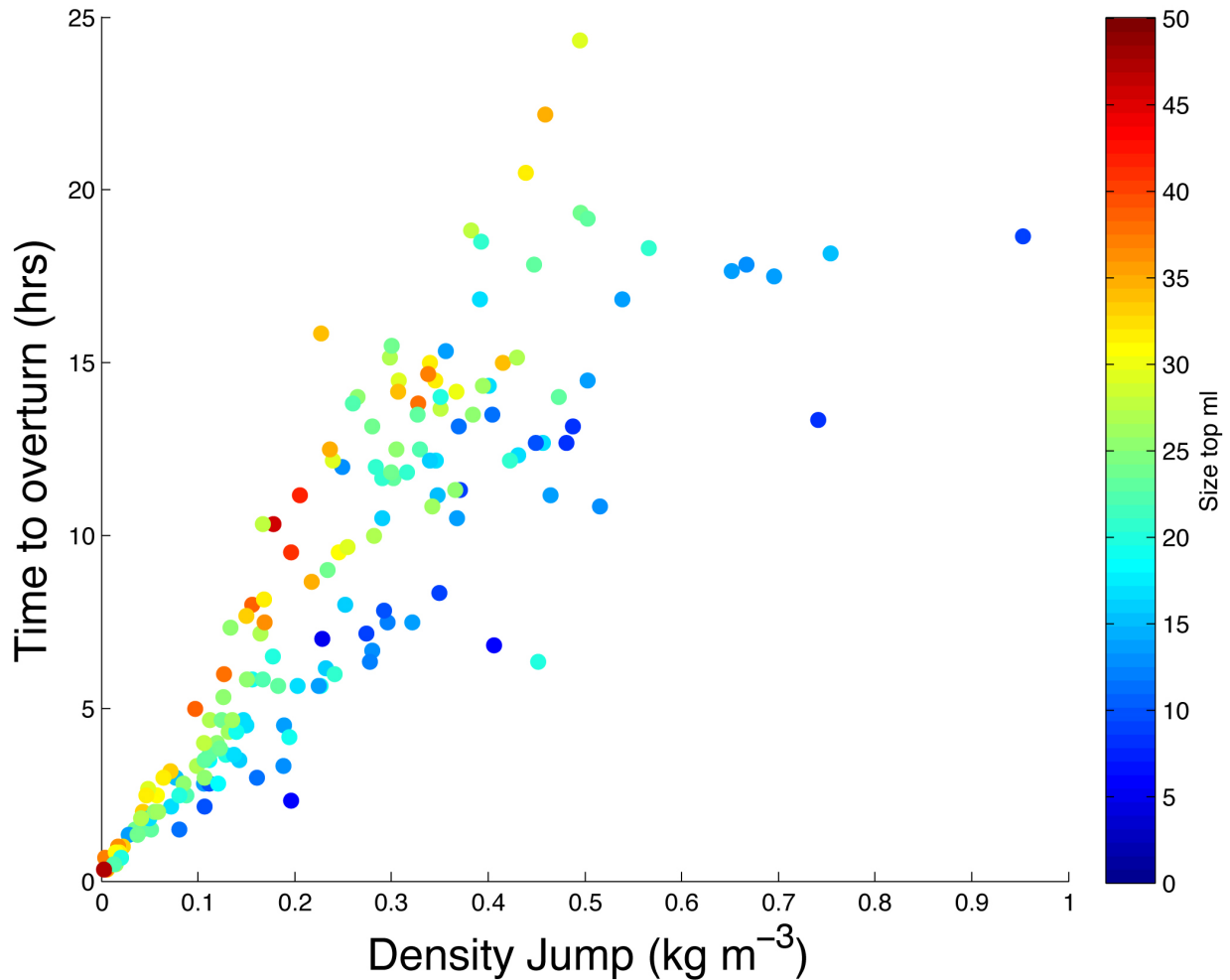


**Figure 10:** Relationship between overturn time and the density jump between the two mixed layers, for the stations containing newly ventilated winter water. The color denotes the height of the surface mixed layer. (We note that three stations whose overturn time was greater than 25 hours are not shown in the figure.)

To quantify this further, we defined an “area” parameter  $a = (\text{density jump}) \times (\text{thickness of the top mixed layer})$  which takes into account both of these characteristics of the profile. This parameter was calculated for each station and compared to the overturn time given by the coupled model (Figure 11). As seen, there is a strong correlation between these two variables, ( $r=0.92$ ). This provides a means to better understand which profiles are poised to overturn the fastest and the time scales associated with the homogenization of the water column.

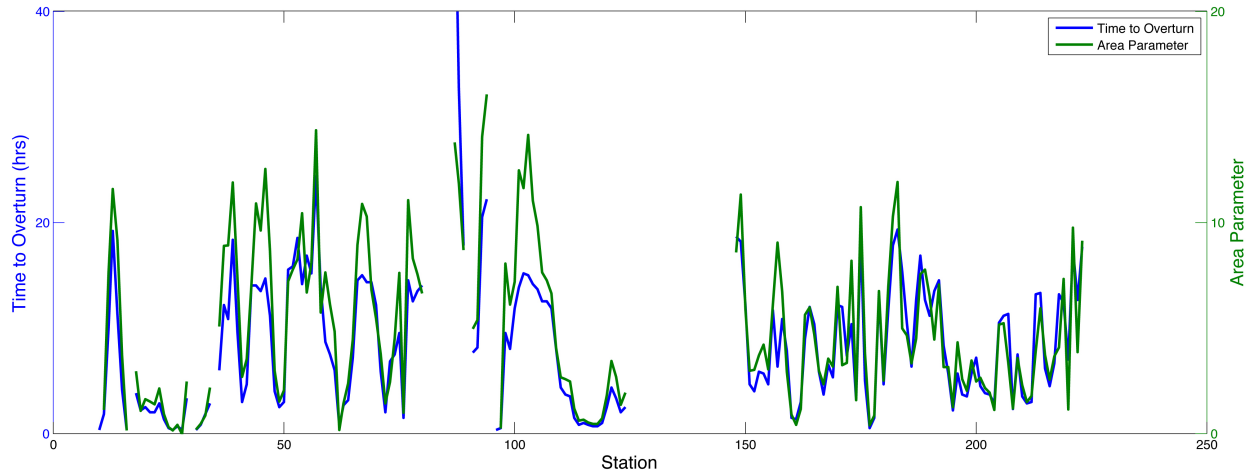


**Figure 11:** Relationship between overturn time (blue) and the value of the area parameter  $a$  (green) for the stations containing newly ventilated winter water.

### 4.3 Transformation by polynyas versus small leads

It has been previously documented that NVWW can be transformed in large polynyas (Weingartner et al., 1998; Itoh et al., 2012; Pickart et al., 2016). The results presented above indicate that, on average, the stations on the shelf during our survey would be overturned in less than 10 hours using realistic atmospheric forcing. Furthermore, we sampled 7 profiles that were homogenized to within  $0.01 \text{ kg m}^{-3}$  in an area of heavy ice cover with only small leads and openings in the sea ice. This strongly suggests that NVWW is modified outside of large polynyas. The next question is, can the degree of such transformation be comparable to that which occurs in polynyas? To assess this, we compared the salinity of the NVWW measured during our cruise along the central flow pathway to that recorded by moorings earlier in the year in Bering Strait in order to determine if salinization took place on the shelf – and, if so, to see if this could be explained solely by polynya activity or whether salinization within leads was needed as a mechanism for elevated salinity values.

We used the same approach as that employed by Pickart et al. (2016) in their investigation of winter water transformation on the Chukchi shelf. First, we identified the stations along the central flow pathway, i.e. the branch that extends around the north side of Hanna Shoal (Figure 8). The average salinity of the NVWW in the surface mixed layer for the parts of the five

transects that crossed the pathway reveals a marked decrease progressing northwards (Figure 12). Using an average advective speed of  $\sim 9$  cm/s, we traced these parcels back in time to when they would have passed through Bering Strait, and compared the mixed layer salinities to the salinity timeseries at mooring A3 in the strait (the location of the mooring is marked in Figure 12). We tried a range of advective speeds, and a value of  $9.2 \text{ cm s}^{-1}$  resulted in the most sensible results in terms of the relationship between the shipboard data and the mooring record. In light of the ADCP flow speeds (Figure 8) and their uncertainty (see section 2.1), such a value is reasonable (also keep in mind the large distance from Bering Strait to the CC line for which we have no velocity measurements). This is also close to the optimal advective speed of  $10.5 \text{ cm s}^{-1}$  determined by Pickart et al. (2016) for the same pathway.

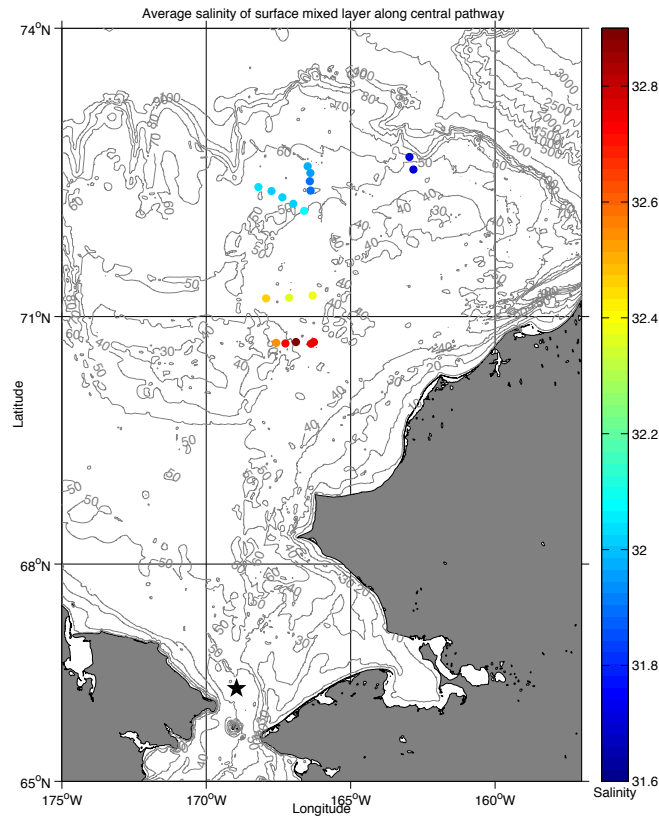


**Figure 12:** Average salinity (color) of the surface mixed layer for the stations along the central flow pathway. The location of the Bering Strait mooring A3 is denoted by the black star.

Our results indicate that the salinities at the three northern transects match the Bering Strait timeseries, but the values at the two southern transects are saltier by  $\sim 0.15$ . To determine if this difference can be explained by salinization within polynyas, we used the daily AMSR-2 satellite product to document the ice concentration following five parcels leaving Bering Strait between late-February and early-April and traveling northward through the Central Channel. The five parcels in question are those that would end up at the five locations respectively in the central pathway (Figure 12) at the time of sampling of the given transect. This revealed that the first four parcels encountered heavy ice concentration, between 90% and 100% (except for a brief period at the beginning of the record, Figure 13). Only the final parcel – the one sampled at the second transect – passed through a polynya. In particular, it encountered the western end of the Cape Lisburne polynya several times before reaching its sampling point (corresponding to the large reductions in ice concentration in Figure 13).

Using the data set collected in 2011, Pickart et al. (2016) also determined that NVWW traveling along the central pathway was salinized within the Cape Lisburne polynya. They used the same polynya model as that employed above to estimate the brine rejection following parcels along the pathway, and found that the predicted salinity increase between Bering Strait and the measurement locations on the shelf was sufficient to explain the observed changes. We use the same methodology here on the final parcel which passed through the Cape Lisburne polynya. Following Pickart et al. (2016), we assume that the parcel is at the freezing point and then calculate the salinization each day that the parcel experiences ice concentrations below 80%. We use a heat flux of  $150 \text{ W/m}^2$  (consistent with the above observations). The result indicates that the salinity of this parcel is increased by 0.15, corresponding to the observed increase. Hence it appears that the same process that took place in 2011 also occurred in 2014. However, the increase in salinity at the first transect in Figure 13 (the Central Channel transect), which was also 0.15, cannot be similarly explained since the water in question did not encounter any polynyas during its transit from Bering Strait to the measurement location. This implies that salinization within small leads in consolidated pack ice can be just as effective as that occurring in larger polynyas.

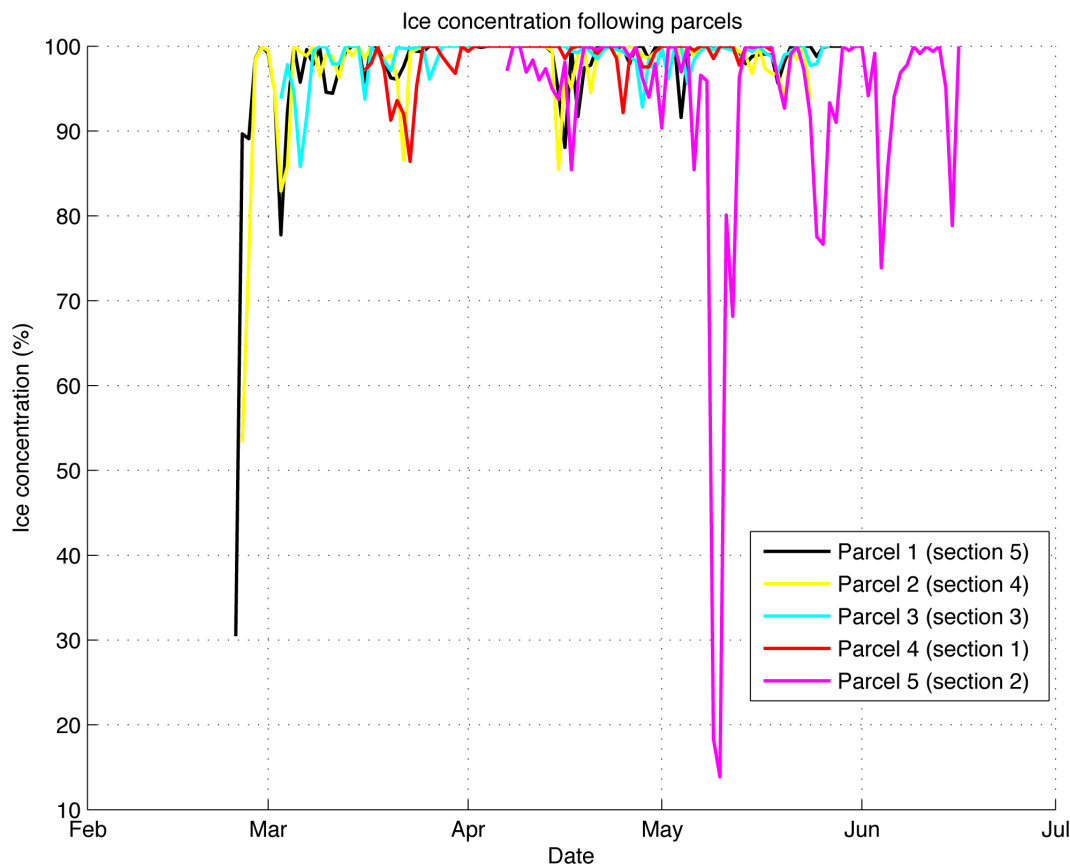


**Figure 13:** Ice concentration from AMSR-2 following each of the five parcels emanating from Bering Strait (see text for details).

#### 4.4 Ramifications for primary production

It is well known that nutrient-enriched NVWW flows into the Chukchi Sea through Bering Strait during the winter and early spring (e.g. Woodgate et al., 2005). This winter water is formed (and salinized) in the Bering Sea during ice formation (e.g. Muench et al., 1988) and flows along the major circulation pathways on the Chukchi shelf. In addition, the water can be further modified on the shelf within polynyas (the Cape Lisburne polynya and the Northeast Chukchi Sea polynya). This notion is consistent with our observations, which showed enhanced levels of nitrate and salinity in both the central pathway and coastal pathway (and a smaller pathway through the ridge between Herald and Hanna Shoals). However, our data suggest that there is another paradigm by which NVWW fills the remainder of the Chukchi shelf – outside of the pathways and away from large polynyas. The evidence presented above implies that winter

water can be formed and/or further transformed within small leads and openings in the pack ice. The polynya-PWP model indicated that homogenization of the water column can occur quickly for realistic atmospheric forcing, and we sampled multiple instances of a uniform density profile. Furthermore, the presence of small, re-freezing leads was common throughout our study area.

It is evident that during the cold season, whenever a small hole in the ice opens up, it does not take much for convection to erode the weak stratification and reach the bottom. Importantly, when this happens the nutrients in and above the sediments will be stirred into the water column. Vertical export of carbon is strong in the Chukchi Sea, since the zooplankton are not able to consume all of the primary production that occurs each summer (Campbell et al., 2009). The remaining carbon sinks to the seafloor where it is remineralized both by microbial activity and cycling by the benthic macrofauna, resulting in high levels of inorganic nutrients in the pore water (Mathis et al., 2014). Hence, the convection on the shelf during winter is able to tap these nutrients and transport them to the surface layer where they are available for primary production the following summer.

This local source of nutrients, together with the remote supply advected through Bering Strait, is apparently enough to fill most of the Chukchi Sea with high concentrations of nitrate (which is the limiting nutrient for primary production on the shelf; Codispoti et al., 2005). The more active the convection, the saltier the water will be and the more sustained the vertical transport of nitrate will be. This is consistent with the high correlation between these two variables seen in our data set (discussed as well in Arrigo et al., submitted). Overall, this emphasizes the importance of a dynamic ice pack (i.e. lots of openings) and the fact that the Chukchi Sea is shallow (i.e. the ability for convection to reach the bottom) for the seasonal occurrence of phytoplankton blooms throughout the shelf.

## **5. Atmospheric setting**

During the early-summer 2011 survey of the Chukchi Sea, a massive under-ice bloom was serendipitously found on the northern part of the shelf (Arrigo et al., 2014). This discovery motivated the 2014 survey described here to investigate more thoroughly the conditions surrounding such under-ice blooms. Using satellite data, Lowry et al. (2014) deduced that these blooms are common in the Chukchi Sea, and the main goal of the 2014 field program was to

document this using in-situ data. As demonstrated by Arrigo et al. (2014), one of the important factors leading to the development of under-ice blooms is the presence of melt ponds on the ice. This enables much more of the incident sunlight to enter the water column due to the decreased index of refraction between the air and water.

Unfortunately, no significant under-ice bloom activity was observed during the cruise, despite the fact that the Chukchi Sea was favorably preconditioned for phytoplankton growth due to the large amount of nutrient-rich NVWW present on the shelf. We attribute this in part to the fact that no melt ponds formed on the northeast part of the shelf during the measurement period. Recall, however, that there were plenty of leads present which would allow most of the incident sunlight to enter the water column within these small features. This would seemingly promote phytoplankton growth. However, as discussed above, the leads were often re-freezing (particularly during the first part of the cruise) and active convection was likely taking place. The associated vertical currents would thus convect the phytoplankton away from the surface layer before a bloom could develop. Lowry et al. (submitted) present compelling evidence that this was indeed the case.

The lack of under-ice blooms during the SUBICE cruise motivates consideration of the atmospheric conditions to determine if they played a role in hindering the blooms. In particular, we seek to explain why the onset of melt ponds might have been delayed in spring 2014. Using the ERAI reanalysis data, we characterized the conditions over the course of the cruise and compared this to the 36-year climatology (1979-2014). We considered both the 2-m air temperature and the meridional winds averaged within a box over the Chukchi Sea (Figure 14, yellow box). Specifically, the daily mean values were calculated for May and June 2014 as well as the climatological daily means over this two-month period. Single spectrum analysis (SSA) was then used to determine the low-frequency signals (see Hassani, 2007; Lin et al., 2016). The resulting timeseries are shown in Figure 15.

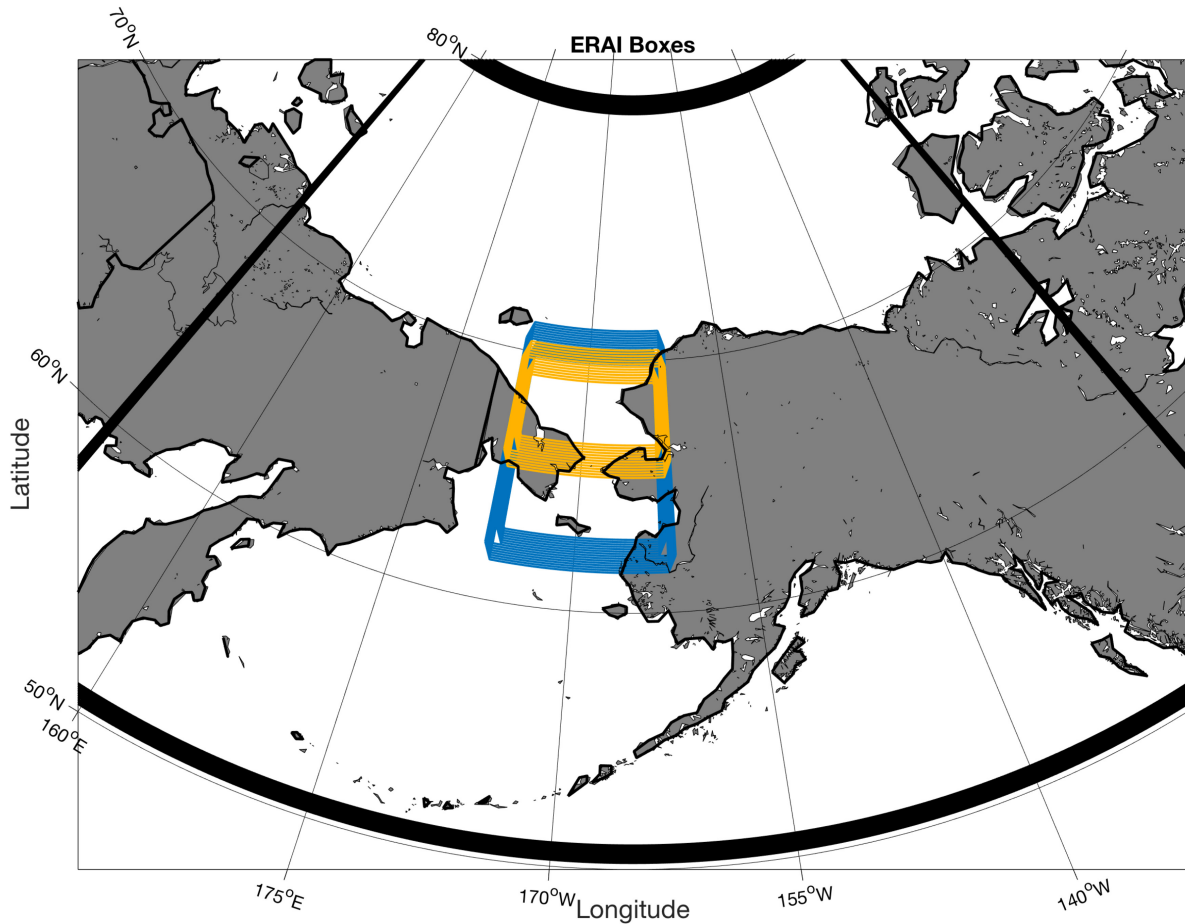


**Figure 14:** Boxes showing the different domains used for the ERAI analyses (see text).

Climatologically, the air temperature over the Chukchi Sea rises above freezing around the first of June, reaching 4°C by the end of the month (Figure 15a). The meridional winds are typically weak during June (Figure 15b); thus, solar radiation is the main reason for the increased air temperatures (versus advection). This warm air would promote the formation of melt ponds. The conditions in 2014 were markedly different than the norm (Figure 15c,d). While the short term fluctuations were larger (not surprisingly since this is a single year versus a long-term average), the smoothed trends were different as well. This is highlighted in Figures 15e,f which compare the SSA curves between the climatology and 2014. One sees that, for roughly the first three weeks of May, the air temperature in 2014 was much warmer than normal. This was clearly the result of anomalous southerly winds advecting warm air from the south during that time.

However, the abrupt change in winds in late-May from southerly to mostly northerly caused the air temperatures over the next several weeks to be 0.5 – 1°C colder than normal.

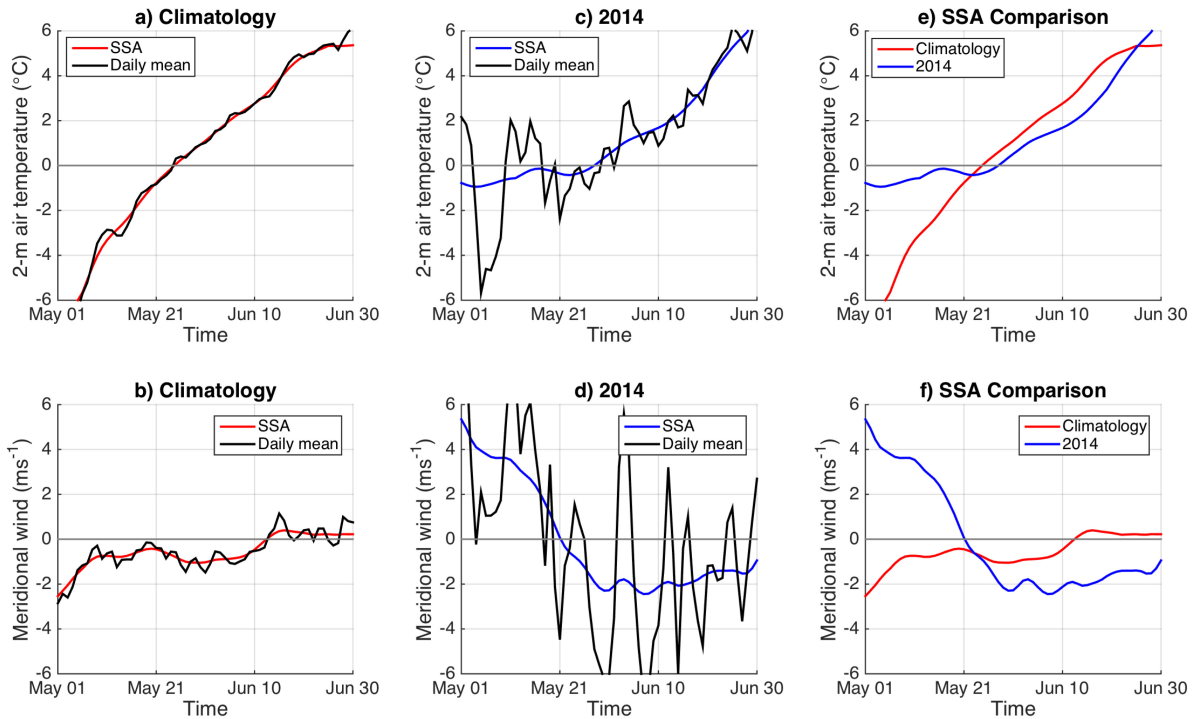


**Figure 15:** Timeseries of 2-m air temperature (top row) and 10-m meridional wind (bottom row) from ERAI, averaged over the region denoted by the yellow box in Figure 14. The black curves are the mean daily values, and the red and blue curves are the corresponding SSA reconstructions. The climatological timeseries are shown in the first column, the 2014 timeseries in the second column, and the comparison between the SSA reconstructions in the third column.

The warmer than average conditions during the first part of May were due to a pronounced region of high pressure situated in the Bering Sea, drawing warm air from the south (Figure 16, top panel). This is quite different than the normal scenario at this time of year, which is depicted by the 36-year composite fields for the period May 1-22 (Figure 16, middle panel). One sees that typically there is an Aleutian Low signature in the Bering Sea and a strong Beaufort High, which together result in northeasterly winds in the Chukchi Sea. The anomaly fields (Figure 16, bottom panel) show a strong dipole between the Bering Sea and Canada Basin which led to above average air temperatures throughout the Chukchi and Beaufort Seas. Such high pressure in the Bering Sea is not common at this time of year; over the 36-year ERAI record these conditions occurred only 7 times.

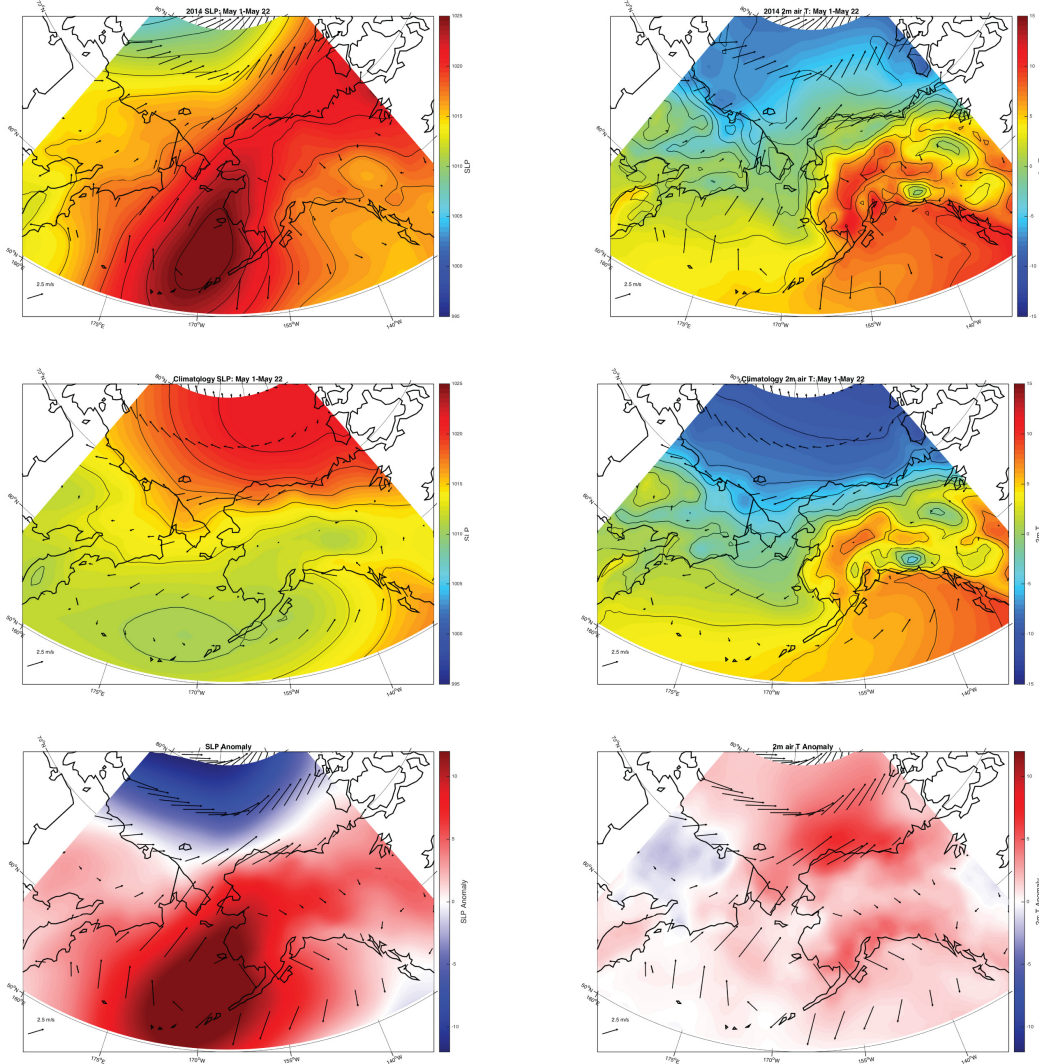


**Figure 16:** Top row: atmospheric conditions during 1-22 May 2014 from ERAI. The left-hand panel is sea level pressure (mb, color and contours) and 10m wind vectors (m/s, see the key). The right-hand panel is 2m air temperature ( $^{\circ}\text{C}$ , color and contours) and 10m wind vectors. Middle row: climatological conditions over the 36-year ERAI record for 1-22 May. The variables are the same as the top row. Bottom row: Anomaly fields (2014 minus climatology).

The colder than normal conditions from the end of May through June 2014 were associated with the presence of the Beaufort High in conjunction with low pressure over the Alaskan continent (Figure 17, top panel). This led to northerly winds throughout the Chukchi Sea which advected cold air from the north. However, comparing this to the climatology for the period May 23 – June 30 (Figure 17, middle panel), it is evident that these were not especially unique conditions. This is verified by the anomaly fields (Figure 17, bottom panel), which show

generally weak SLP signals and only moderately strong wind vectors out of the north. Nonetheless, this resulted in anomalously cold air temperatures throughout the Chukchi Sea.

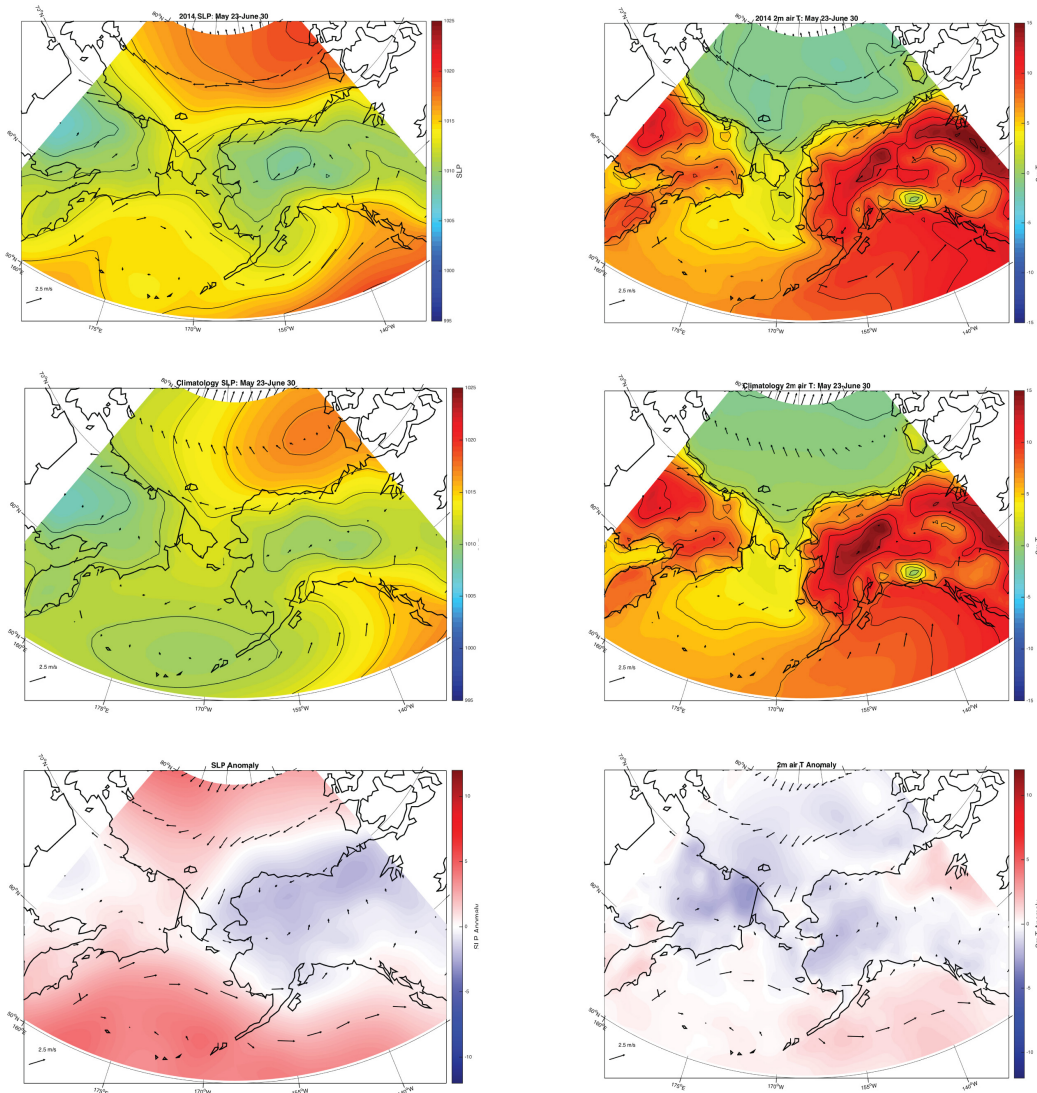


**Figure 17:** Same as Figure 16 for the period 23 May – 30 June.

Typically, melt ponds begin to form in the Chukchi Sea around the first of June (C. Polashenski, Pers. Comm., 2014). This is consistent with the climatological air temperature record which rises above freezing at about this time (Figure 15a). Despite the fact that the air temperatures were significantly warmer in early May 2014, they generally stayed below freezing and were not enough to initiate the ponding. However, the subsequent cold conditions through much of June were evidently able to delay it. Interestingly, the transition to above-freezing temperatures in 2014 happened just a few days later than the climatology, around 1 June (this is

when the heat flux decreased abruptly, Figure 9). Hence the main factor delaying melt pond formation was not an extended period of sub-freezing temperatures, but rather the advection of above-freezing, colder than normal air from the north that counteracted the solar heating during this time.

The importance of ponding for the initiation of under-ice blooms, together with the impact of the atmospheric circulation patterns on the air temperatures of the Chukchi Sea demonstrated above for 2014, motivates investigation of the year-to-year variation in the transition from sub-freezing to above-freezing conditions over the 36-year ERAI record. To do this we constructed a timeseries of 2-m air temperature for the period of May-June for each year, where the temperature was averaged over a box covering the northern Bering and southern Chukchi Seas (Figure 14, blue box). The onset of ice melt was defined as the point where the air temperature stayed above freezing for three consecutive days, and subsequently only dropped below freezing for a maximum of 6 hours at a time for the remainder of the timeseries.

The mean onset date was 31 May, with a standard deviation of about a week (6.6 days). The earliest onset occurred on 16 May (1997) and the latest on 18 June (1985). There was no trend over the 36-year period. We made composite fields for the extreme early onset years as well as the extreme late onset years (i.e. beyond  $\pm 1$  standard deviation from the mean onset date). Specifically, we averaged the conditions over the two weeks prior to the onset in each case, and compared this to the climatological conditions around that time. Notably, this did not reveal any indication of persistent advection of warm or cold air that might help explain the variation in onset times. This implies that year-to-year changes in the radiative flux balance is the dominant driver of this variability. It is important to note, however, that changes in the transition from sub-freezing to above-freezing air temperature alone does not dictate the ponding of ice; for instance, snow depth plays an important role. Also, keep in mind that 2014 was a normal year with regard to transition time, yet ponding was delayed in part due to the atmospheric circulation.

## **6. Summary**

We have presented data from a broad-scale hydrographic survey of the Chukchi Sea carried out in late-spring 2014. The measurement domain covered much of the northeast shelf,

and more than 96% of the water sampled on the shelf was newly ventilated winter water (NVWW). Nearly all of the hydrographic profiles sampled on the shelf consisted of a two-layer structure, with a surface mixed layer and bottom boundary layer separated by a weak density interface. The saltiest (densest) NVWW tended to be in the flow pathways on the shelf, likely advected there from the Bering Sea where winter water is known to be formed. However, away from the pathways the NVWW was also found in abundance, suggesting that the entire Chukchi Sea is filled with winter water at the end of the cold season.

The fact that NVWW was found in regions of highly consolidated pack-ice, outside of the flow pathways and away from known polynyas, suggests a new paradigm for the formation/transformation of this water mass. We argue that winter water is formed throughout the Chukchi shelf via convection within small leads and openings. Our study domain was filled with such small leads – many of them re-freezing – and we sampled profiles with a uniform density structure from top to bottom. Using the output of a polynya model implemented with a realistic heat flux to drive a one-dimensional mixing model, we demonstrated that, on average, the two-layer hydrographic profiles measured on the cruise would become completely homogenized within 8 hours as a result of the brine rejection. We also showed that the salinity signals of the NVWW along the central shelf pathway could not be explained solely by advection from Bering Strait or via modification within large polynyas. These results reinforce our assertion that convection in leads is an important mechanism forming NVWW on the Chukchi shelf.

When the convection reaches the bottom, this stirs regenerated nutrients from the sediments into the water column. This can explain the fact that nitrate concentrations were high throughout our study domain. It is also consistent with the statistically significant correlation between the salinity of NVWW and its nitrate concentration, the idea being that continued brine rejection increases the convective activity, which is more effective for fluxing nutrients upwards from the bottom. Therefore, the presence of small holes in the ice, together with the fact that the Chukchi Sea is generally shallow, could be one of the main reasons for the high level of primary production on the shelf – so long as there is significant vertical export of carbon to the sea floor following the annual summer blooms.

Despite the favorable “initial condition” of high nitrate in the surface water throughout our study domain, we did not observe any under-ice blooms during the five-week cruise. This was attributed to the fact that melt ponds did not develop during our measurement period. Using the ERAI atmospheric reanalysis fields we demonstrated that northerly winds commencing in late-May advected cold air from the north into the Chukchi Sea, which kept air temperatures 0.5 – 1°C colder than normal. This likely counteracted the radiative warming at this time and delayed the ponding. While anomalous atmospheric circulation patterns can influence air temperatures in the Chukchi Sea, which happened both early in the cruise (warming) and late in the cruise (cooling), such advection does not appear to drive the year-to-year variability in the transition from sub-freezing to above-freezing conditions on the Chukchi shelf. Further work is required to explain why the melt onset times change by up to a month in this region.

### **Acknowledgements**

The authors are indebted to Commanding Officer John Reeves, Executive Officer Gregory Stanclik, Operations Officer Jacob Cass, and the entire crew of the USCGC *Healy*, for their hard work and dedication in making the SUBICE cruise a success. We also acknowledge Scott Hiller for his assistance with *Healy's* meteorological data. Funding for AP, RP, CN, and FB was provided by the National Science Foundation (NSF) under grant PLR-1303617. KM was funded by the Natural Sciences and Engineering Research Council of Canada. KV acknowledges the Bergen Research Foundation. KA was supported by NSF grant PLR-1304563.

### **References**

- Aagaard, K., 1984. The Beaufort Undercurrent. The Alaskan Beaufort Sea: Ecosystems and Environments. Academic Press, New York, pp. 47–71.
- Aagaard, K., Roach, A.T., 1990. Arctic Ocean-shelf exchange: measurements in barrow canyon. J. Geophys. Res. 95 (C10), 18163–18175, URL <http://dx.doi.org/10.1029/JC095iC10p18163>.
- Aksenov, Y., Ivanov, V. V., Nurser, A.J.G., Bacon, S., Polyakov, I. V., Coward, A.C., Naveira-Garabato, A.C., Beszczynska-Moeller, A., 2011. The arctic circumpolar boundary current. J. Geophys. Res. Ocean. 116, 1–28.
- Armstrong, F., Stearns, C.R., Strickland, J., 1967. The measurement of upwelling and subsequent biological process by means of the Technicon Autoanalyzer® and associated equipment. Deep-Sea Res. 14, 381-389. [http://dx.doi.org/10.1016/0011-7471\(67\)900890084](http://dx.doi.org/10.1016/0011-7471(67)900890084).
- Arrigo, K.R., Perovich, D.K., Pickart, R.S., Brown, Z.W., van Dijken, G.L., Lowry, K.E., Mills, M.M., Palmer, M.A., Balch, W.M., Bates, N.R., Benitez-Nelson, C.R., Brownlee, E., Frey,

- K.E., Laney, S.R., Mathis, J., Matsuoka, A., Greg Mitchell, B., Moore, G.W.K., Reynolds, R.A., Sosik, H.M., Swift, J.H., 2014. Phytoplankton blooms beneath the sea ice in the Chukchi Sea. *Deep- Sea Res. II* 105, 1–16, URL <http://www.sciencedirect.com/science/article/pii/S0967064514000836>.
- Arrigo, K.R., M. M. Mills<sup>1</sup>, G.L. van Dijken, K.E. Lowry, R.S. Pickart, and R. Schlitzer. Late spring nitrate distributions beneath the ice-covered Chukchi shelf. *Geophysical Research Letters*, submitted.
- Beitsch, A., Kaleschke, L., Kern, S., 2014. Investigating high-resolution AMSR2 sea ice concentrations during the February 2013 fracture event in the Beaufort Sea. *Remote Sens.* 6, 3841–3856.
- Bourke, R.H., Paquette, R.G., 1976. Atlantic water on the Chukchi Shelf. *Geophysical Research Letters* 3, 629–632.
- Brugler, E.T., Pickart, R.S., Moore, G.W.K., Roberts, S., Weingartner, T.J., Statscewich, H., 2014. Seasonal to interannual variability of the pacific water boundary current in the Beaufort Sea. *Progr. Ocean.* 127, 1–20. <http://dx.doi.org/10.1016/j.pocan.2014.05.002>.
- Campbell, R.G., Sherr, E.B., Ashjian, C.J., Plourde, S. Sherr, B.F., Hill, V., Stockwell, D.A., 2009. Mesozooplankton prey preference and grazing impact in the Western Arctic Ocean. *Deep-Sea Research II* 56: 1274-1289.
- Cavalieri, D.J., Martin, S., 1994. The contribution of Alaskan, Siberian, and Canadian coastal polynyas to the cold halocline of the Arctic Ocean. *Journal of Geophysical Research* 99, 18, 343–18, 362.
- Chang, E.K.M., 2009. Are band-pass variance statistics useful measures of storm track activity? Re-examining storm track variability associated with the NAO using multiple storm track measures. *Clim. Dyn.* 33, 277–296. doi:10.1007/s00382-009-0532-9
- Codispoti, L.A., Flagg, C., Kelly, V., Swift, J.H., 2005. Hydrographic conditions during the 2002 SBI process experiments. *Deep-Sea Research II*, 52, 3199–3226.
- Corlett, W.B., Pickart, R.S., Submitted. The Chukchi Slope Current. *Progress in Oceanography*.
- Dee, D.P., Uppala, S.M., Simmons, A.J., Berrisford, P., Poli, P., Kobayashi, S., Andrae, U., Balmaseda, M.A., Balsamo, G., Bauer, P., Bechtold, P., Beljaars, A.C.M., van de Berg, L., Bidlot, J., Bormann, N., Delsol, C., Dragani, R., Fuentes, M., Geer, A.J., Haimberger, L., Healy, S.B., Hersbach, H., Hólm, E. V., Isaksen, L., Kållberg, P., Köhler, M., Matricardi, M., McNally, A.P., Monge-Sanz, B.M., Morcrette, J.-J., Park, B.-K., Peubey, C., de Rosnay, P., Tavolato, C., Thépaut, J.-N., Vitart, F., 2011. The ERA-Interim reanalysis: Configuration and performance of the data assimilation system. *Q. J. R. Meteorol. Soc.* 137, 553–597. doi:10.1002/qj.828
- Fairall, C.W., Bradley, E.F., Hare, J.E., Grachev, A.A., Edson, J.B., 2003. Bulk parameterization of air-sea fluxes: Updates and verification for the COARE algorithm. *J. Clim.* 16, 571–591. doi:10.1175/1520-0442(2003)016<0571:BPOASF>2.0.CO;2
- Gong, D., Pickart, R.S., 2015. Summertime circulation in the eastern Chukchi Sea. *Deep-Sea Research II* 118, 18-31.
- Hassani, H., 2007. Singular spectrum analysis: Methodology and comparison. *J. Data Sci.* 5, 239–257.
- Hill, V., Cota, G., 2005. Spatial patterns of primary production in the Chukchi Sea in the spring and summer of 2002. *Deep- Sea Research II*, this issue [doi:10.1016/j.dsr2.2005.10.001].
- Itoh, M., Pickart, R.S., Kikuchi, T., Fukamachi, Y., Ohshima, K.I., Simizu, D., Arrigo, K.R., Vagle, S., He, J., Ashjian, C., Mathis, J.T., Nishino, S., Nobre, C., 2015. Water prop- erties,

- heat and volume fluxes of Pacific water in Barrow Canyon during summer 2010. *Journal of Geophysical Research* 102, 43–54.
- Itoh, M., Shimada, K., Kamoshida, T., McLaughlin, F., Carmack, E.C., Nishino, S., 2012. Interannual variability of PWV in flow through Barrow Canyon from 2000 to 2006. *J. Ocean*. <http://dx.doi.org/10.1007/s10872-012-0120-1>
- Kalnay, E., Kanamitsu, M., Kistler, R., Collins, W., Deaven, D., Gandin, L., Iredell, M., Saha, S., White, G., Woollen, J., Zhu, Y., Leetmaa, A., Reynolds, R., Chelliah, M., Ebisuzaki, W., Higgins, W., Janowiak, J., Mo, K.C., Ropelewski, C., Wang, J., Jenne, R., Joseph, D., 1996. The NCEP/NCAR 40-Year Reanalysis Project. *Bull. Am. Meteorol. Soc.* 77, 437–471. doi:10.1175/1520-0477(1996)077<0437:TNYP>2.0.CO;2
- Karcher, M., Kauker, F., Gerdes, R., Hunke, E., Zhang, J., 2007. On the Dynamics of Atlantic Water Circulation in the Arctic Ocean. *J. Geophys. Res.* 112.
- Kobayashi, S., Ota, Y., Harada, Y., Ebata, A., Moriya, M., Onoda, H., Onogi, K., Kamahori, H., Kobayashi, C., Endo, H., Miyaoka, K., Takahashi, K., 2015. The JRA-55 Reanalysis: General Specifications and Basic Characteristics. *J. Meteorol. Soc. Japan. Ser. II* 93, 5-48. doi:10.2151/jmsj.2015-001
- Ladd, C., Mordy, C.W., Salo, S.A., Stabeno, P.J., 2016. Winter water properties and the Chukchi Polynya. *J. Geophys. Res. Ocean.* 121, 5516–5534.
- Lentz, S., Trowbridge, J., 1991. The Bottom Boundary Layer over the Northern Californian Shelf. *J. Phys. Oceanogr.* doi:10.1175/1520-0485(1991)021<1186:TBBLOT>2.0.CO;2
- Lin, P., Pickart, R. S., Stafford, K. M., Moore, G. W. K., Torres, D. J., Bahr, F., Hu, J., 2016. Seasonal variation of the Beaufort shelfbreak jet and its relationship to Arctic cetacean occurrence, *J. Geophys. Res. Oceans*, 121, doi:10.1002/2016JC011890.
- Lowry, K.E., Pickart, R.S., Mills, M.M., Pacini, A., Selz, V., Lewis, K.M., Submitted. Under-ice phytoplankton bloom dynamics controlled by spring convective mixing in refreezing leads of open water. *J. Geophys. Res. Ocean.* 1–47.
- Lowry, K.E., Pickart, R.S., Mills, M.M., Brown, Z.W., van Dijken, G.L., Bates, N.R., Arrigo, K.R., 2015. Influence of winter water on phytoplankton blooms in the Chukchi Sea. *Deep-Sea Research II* 118, 53–72.
- Lowry, K.E., van Dijken, G.L., Arrigo, K.R., 2014. Evidence of under-ice phytoplankton blooms in the Chukchi Sea from 1998 to 2012. *Deep-Sea Research II* 105, 105–117. doi:10.1016/j.dsr2.2014.03.013
- Mathis, J.T., Grebmeier, J.M., Hansell, D.A., Hopcroft, R.R., Kirchman, D., Lee, S.H., Moran, S.B., 2014. Carbon Biogeochemistry of the Western Arctic: Production, Export and Ocean Acidification. In: Grebmeier JM, Maslowski W (eds) *The Pacific Arctic Region: Ecosystem Status and Trends in a Rapidly Changing Environment*, Springer, Dordrecht, p. 223-268.
- Mathis, J.T., Pickart, R.S., Hansell, D.A., Kadko, D., Bates, N.R., 2007. Eddy transport of organic carbon and nutrients from the Chukchi Shelf: Impact on the upper halocline of the western Arctic Ocean. *J. Geophys. Res.*, 112, doi:10.1029/2006JC003899.
- Mesinger, F., DiMego, G., Kalnay, E., Mitchell, K., Shafran, P.C., Ebisuzaki, W., Jović, D., Woollen, J., Rogers, E., Berbery, E.H., Ek, M.B., Fan, Y., Grumbine, R., Higgins, W., Li, H., Lin, Y., Manikin, G., Parrish, D., Shi, W., 2006. North American regional reanalysis. *Bull. Am. Meteorol. Soc.* 87, 343–360. doi:10.1175/BAMS-87-3-343
- Muench, R.D., Schumacher, J.D., Salo, S.A., 1988. Winter currents and hydrographic conditions on the northern central Bering Sea shelf. *J. Geophys. Res.* 93 (C1), 516–526. <http://dx.doi.org/10.1029/JC093iC01p00516>.

- Muench, R.D., Gunn, J.T., Whitley, T.E., Schlosser, P., Smethie Jr., W., 2000. An Arctic Ocean cold core eddy. *Journal of Geophysical Research* 105, 23,997–24,006.
- Nikolopoulos, A., Pickart, R.S., Fratantoni, P.S., Shimada, K., Torres, D.J., Jones, E.P., 2009. The western Arctic boundary current at 152°W: Structure, variability, and transport. *Deep Sea Res., Part II*, 56, 1164–1181.
- Padman, L., Erofeeva, S., 2004. A barotropic inverse tidal model for the Arctic Ocean. *Geophysical Research Letters* 31, L02303, doi:10.1029/2003GL019003.
- Paquette, R.G., Bourke, R.H., 1974. Observation on the coastal current of Arctic Alaska. *J. Marine Res.* 32, 195-207.
- Paquette, R.G., Bourke, R.H., 1981. Ocean circulation and fronts as related to ice melt-back in the Chukchi Sea. *J. Geophys. Res.* 86 (C5), 4215–4230, URL <http://dx.doi.org/10.1029/JC086iC05p04215>.
- Pickart, R.S., Moore, G.W.K., Mao, C., Bahr, F., Nobre, C., Weingartner, T.J., 2016. Circulation of winter water on the Chukchi shelf in early Summer. *Deep-Sea Research II* 130, 56–75. doi:10.1016/j.dsr2.2016.05.001
- Pickart, R.S., Pratt, L.J., Torres, D.J., Whitley, T.E., Proshutinsky, A.Y., Aagaard, K., Agnew, T.A., Moore, G.W.K., Dail, H.J., 2010. Evolution and dynamics of the flow through Herald Canyon in the western Chukchi Sea. *Deep-Sea Res. II T.* 57 (1–2), 5–26. <http://dx.doi.org/10.1016/j.dsr2.2009.08.002>.
- Pickart, R.S., Torres, D.J., Clarke, R.A., 2002. Hydrography of the Labrador Sea during Active Convection. *J. Phys. Oceanogr.* 32, 428–457. doi:10.1175/1520-0485(2002)032<0428:HOTLSD>2.0.CO;2
- Pickart, R.S., Weingartner, T.J., Pratt, L.J., Zimmermann, S., Torres, D.J., 2005. Flow of winter-transformed Pacific water into the Western Arctic. *Deep-Sea Res. II* 52 (24–26), 3175–3198. <http://dx.doi.org/10.1016/j.dsr2.2005.10.009>.
- Pisareva, M.N., Pickart, R.S., Spall, M.A., Nobre, C., Torres, D.J., Moore, G.W.K., Whitley, T.E., 2015. Flow of Pacific water in the western Chukchi Sea: Results from the 2009 RUSALCA expedition. *Deep-Sea Res. Part I* 105, 53–73. doi:10.1016/j.dsr.2015.08.011
- Price, J.F., Weller, R.A., Pinkel, R., 1986. Diurnal cycling; upper ocean response to heating, cooling and wind mixing. *J. Geophys. Ocean.*
- Rudels, B., Jones, E.P., Schauer, U., Eriksson, P., 2004. Atlantic sources of the Arctic Ocean surface and halocline waters. *Polar Res.* 23, 181–208. doi:10.3402/polar.v23i2.6278
- Shimada, K., Carmack, E.C., Hatakeyama, K., Takizawa, T., 2001. Varieties of shallow temperature maximum waters in the western Canadian basin of the Arctic ocean. *Geophysical Research Letters* 28, 3441–3444.
- Spall, M.A., 2007. Circulation and water mass transformation in a model of the Chukchi Sea. *J. Geophys. Res.* 112 (C5) 2007/05/11. <http://dx.doi.org/10.1029/2005JC003364>.
- Spall, M.A., Pickart, R.S., Fratantoni, P.S., Plueddemann, A.J., 2008. Western Arctic shelfbreak eddies: formation and transport. *J. Phys. Oceanogr.* 38 (8), 1644–1668 2008/08/01. URL <http://dx.doi.org/10.1175/2007JPO3829.1>.
- Steele, M., Morison, J., Ermold, W., Rigor, I., Ortmeier, M., Shimada, K., 2004. Circulation of summer Pacific halocline water in the Arctic Ocean. *J. Geophys. Res.* 109 (C2) 2004/02/26. URL <http://dx.doi.org/10.1029/2003JC002009>.
- Timmermans, M.-L., Toole, J., Proshutinsky, A., Krishfield, R., Plueddemann, A., 2008. Eddies in the Canada Basin, Arctic Ocean, Observed from Ice-Tethered Profilers. *J. Phys. Oceanogr.* 38, 133–145. doi:10.1175/2007JPO3782.1

- Trowbridge, J.H., Lentz, S.J., 1991. Asymmetric Behavior of an Oceanic Boundary Layer above a Sloping Bottom. *J. Phys. Oceanogr.* doi:10.1175/1520-0485(1991)021<1171:ABOAOB>2.0.CO;2
- von Appen, W.-J., Pickart, R.S., 2012. Two configurations of the Western Arctic Shelfbreak current in summer. *J. Phys. Oceanogr.* 42 (3), 329–351 2011/08/01. URL <http://dx.doi.org/10.1175/JPO-D-11-026.1>.
- Weingartner, T., Danielson, S., Sasaki, Y., Pavlov, V., Kulakov, M., 1999. The Siberian Coastal current: a wind- and buoyancy-forced Arctic coastal current. *Journal of Geophysical Research* 104 (C12), 29697–29713.
- Weingartner, T.J., Cavalieri, D.J., Aagaard, K., Sasaki, Y., 1998. Circulation, dense water formation, and outflow on the northeast Chukchi shelf. *Journal of Geophysical Research* 103, 7647–7661.
- Weingartner, T., Aagaard, K., Woodgate, R., Danielson, S., Sasaki, Y., Cavalieri, D., 2005. Circulation on the north central Chukchi Sea shelf. *Deep- Sea Res. II* . 52 (24–26), 3150–3174. <http://dx.doi.org/10.1016/j.dsr2.2005.10.015>.
- Woodgate, R.A., Aagaard, K., Weingartner, T.J., 2005. A year in the physical oceanography of the Chukchi Sea: moored measurements from autumn 1990–1991. *Deep- Sea Res. II* 52 (24–26), 3116–3149, URL <http://www.sciencedirect.com/science/article/pii/S0967064505002146>.
- Zhao, M., Timmermans, M.-L., Cole, S., Krishfield, R., Proshutinsky, A., Toole, J., 2014. Characterizing the eddy field in the Arctic Ocean halocline. *J. Geophys. Res. Ocean.* 119, 8800–8817. doi:10.1002/2014JC010488
- Zhao, M., Timmermans, M.-L., Cole, S., Krishfield, R., Toole, J., 2016. Evolution of the Eddy Field in the Arctic Ocean’s Canada Basin, 2005-2015. *Geophysical Research Letters* 43. Doi: 10.1002/2016GL069671.
- Zib, B.J., Dong, X., Xi, B., Kennedy, A., 2012. Evaluation and intercomparison of cloud fraction and radiative fluxes in recent reanalyses over the arctic using BSRN surface observations. *J. Clim.* 25, 2291–2305. doi:10.1175/JCLI-D-11-00147.